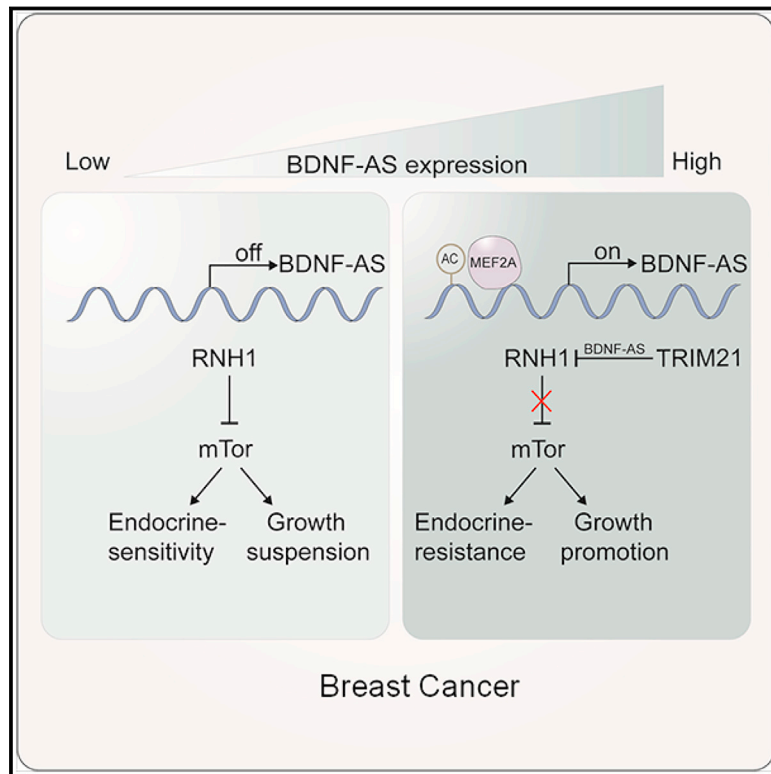


Enhancer-Driven IncRNA BDNF-AS Induces Endocrine Resistance and Malignant Progression of Breast Cancer through the RNH1/TRIM21/mTOR Cascade

Graphical Abstract



Authors

Xiaorong Lin, Xiaoxiao Dinglin, Siting Cao, ..., Qiang Liu, Herui Yao, Hai Hu

Correspondence

yaoherui@163.com (H.Y.), huhai@mail.sysu.edu.cn (H.H.)

In Brief

Epigenomic alterations can give rise to various tumor-promoting properties, including therapeutic resistance of cancer cells. Lin et al. show that the IncRNA BDNF-AS, driven by a MEF2A-regulated enhancer, activates the RNH1/TRIM21/mTOR cascade to induce endocrine resistance and malignant progression of breast cancer.

Highlights

- BDNF-AS induces tamoxifen resistance and malignant progression of breast cancers
- BDNF-AS driven by MEF2A-regulated enhancer acts as scaffold of RNH1/TRIM21
- BDNF-AS activates mTOR pathway by abolishing RNH1-regulated mTOR mRNA decay



Article

Enhancer-Driven lncRNA BDNF-AS Induces Endocrine Resistance and Malignant Progression of Breast Cancer through the RNH1/TRIM21/mTOR Cascade

Xiaorong Lin,^{1,2,4,7} Xiaoxiao Dinglin,^{3,7} Siting Cao,⁵ Senyou Zheng,³ Cheng Wu,⁶ Wenyong Chen,^{1,3} Qingjian Li,³ Qian Hu,³ Fang Zheng,¹ Zhiyong Wu,⁴ De-Chen Lin,¹ Yandan Yao,² Xiaoding Xu,¹ Zhi Xie,⁶ Qiang Liu,^{1,2} Herui Yao,^{1,3,*} and Hai Hu^{1,3,8,*}

¹Guangdong Provincial Key Laboratory of Malignant Tumor Epigenetics and Gene Regulation, Sun Yat-sen Memorial Hospital, Sun Yat-sen University, Guangzhou 510120, People's Republic of China

²Breast Tumor Center, Sun Yat-sen Memorial Hospital, Sun Yat-sen University, Guangzhou 510120, People's Republic of China

³Department of Oncology, Sun Yat-sen Memorial Hospital, Sun Yat-sen University, Guangzhou 510120, People's Republic of China

⁴Diagnosis and Treatment Center of Breast Diseases, Shantou Affiliated Hospital, Sun Yat-sen University, Shantou 515031, People's Republic of China

⁵Department of Endocrinology, The First Affiliated Hospital, Sun Yat-sen University, Guangzhou 510030, People's Republic of China

⁶State Key Laboratory of Ophthalmology, Zhongshan Ophthalmic Center, Sun Yat-sen University, Guangzhou 510663, People's Republic of China

⁷These authors contributed equally

⁸Lead Contact

*Correspondence: yaoherui@163.com (H.Y.), huhai@mail.sysu.edu.cn (H.H.)

<https://doi.org/10.1016/j.celrep.2020.107753>

SUMMARY

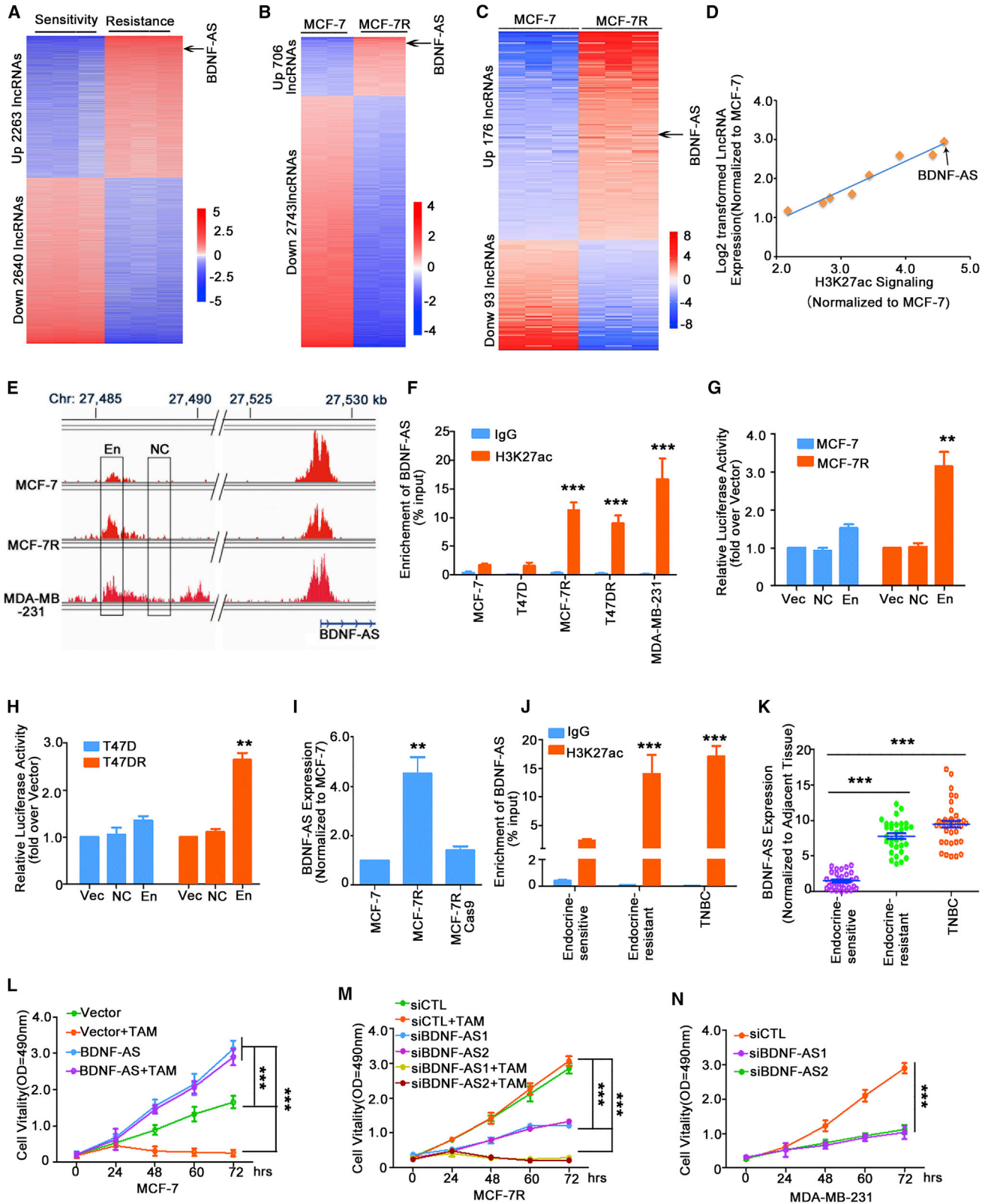
Epigenomic alterations can give rise to various tumor-promoting properties, including therapeutic resistance of cancer cells. Here, we identify an lncRNA, BDNF-AS, whose overexpression is specifically driven by a MEF2A-regulated enhancer in endocrine-resistant and triple-negative breast cancer (TNBC). High levels of BDNF-AS in breast cancer tissues not only feature endocrine resistance in hormone receptor (HR)-positive patients but also correlate with poor outcomes in both HR-positive and TNBC patients. Mechanistically, BDNF-AS acts as a molecular scaffold to promote RNH1 protein degradation via TRIM21-mediated ubiquitination of RNH1 at K225. Subsequently, BDNF-AS abolishes RNH1-regulated and RISC-mediated mTOR mRNA decay, therefore sustaining the activation of mTOR signaling. Importantly, mTOR inhibitor, but not PI3K inhibitor, could reverse tamoxifen resistance induced by the overexpression of BDNF-AS. These results point toward a master regulatory role of an enhancer-activated cascade of BDNF-AS/RNH1/TRIM21/mTOR in endocrine resistance and malignant progression of breast cancer.

INTRODUCTION

Enhancer-related regulations are the major drivers of cell type-specific transcription machinery. In cancer cells, epigenomic regulatory enhancer networks are often rewired by molecular aberrations that collectively lead to the progression of cancers (Chen et al., 2015; Kolch et al., 2015). These processes can generate tumor-specific activation of epigenomic mis-regulation that drives tumorigenesis as well as the development of resistance during treatment (Murakawa et al., 2016). The most recent genome-wide characterization of the human cancer transcriptome has demonstrated that the expression of long non-coding RNA (lncRNA) is among the most pervasive transcriptional changes in cancer (Du et al., 2013; Iyer et al., 2015). Epigenomic regulations are proposed to heritably contribute to the expression patterns of both protein-coding genes (Cedar and Bergman, 2009; Martin and Zhang, 2005) and lncRNAs (Amin et al., 2015; Guttman et al., 2009; Wu et al., 2010), which profoundly affects the behavior of cancers.

Both intrinsic and acquired resistance to endocrine therapies are accountable for relapses in hormone receptor (HR)-positive breast cancer (BC) patients (Dowsett et al., 2015). Clinically, inhibitors of PI3K or mTOR are used to restore the sensitivity toward endocrine therapy, which emphasizes that activation of the PI3K/AKT/mTOR axis plays a critical role in endocrine resistance (AlFakeeh and Brezden-Masley, 2018; Finn et al., 2016). The hyper-activation of this pathway is frequently due to mutations of PI3K and AKT or PTEN loss as well as overexpression of the key regulators of the PI3K/AKT/mTOR cascade. Patients with endocrine resistance with these genomic abnormalities often benefit from the combination treatment of PI3K or mTOR inhibitors with endocrine therapies (AlFakeeh and Brezden-Masley, 2018). On the other hand, many patients without PI3K/AKT genetic alterations also achieved curative effects from treatment with mTOR inhibitors, suggesting that there may be unknown mechanisms that activate the PI3K/AKT/mTOR pathway in endocrine-resistant patients. Moreover, predictive biomarkers





(legend on next page)

of the response to mTOR inhibitors have yet to be discovered (Cristofanilli et al., 2016).

lncRNAs have been reported to be involved in resistance to treatment and malignant progression of cancers (Campos-Parra et al., 2018). However, the key epigenomic alteration-regulated lncRNAs and their consequences in the progression of BC as well as endocrine resistance remain largely uncharacterized. In the present study, we discovered a mechanism whereby the enhancer-activated lncRNA BDNF-AS prevents mTOR mRNA decay, therefore sustaining the activity of mTOR signaling, specifically in endocrine-resistant BCs and triple-negative BCs (TNBCs). Even for PIK3CA-mutated cancer, BDNF-AS overexpression is a predictive marker of endocrine resistance of HR-positive BC and indicates the application of mTOR inhibitor for reversing the resistance.

RESULTS

Epigenomic Activation of BDNF-AS Enhancer Promotes BC Endocrine Resistance and Cancer Cell Proliferation

To investigate whether the dysregulation of lncRNAs was involved in endocrine resistance of BC, the lncRNA microarray was used to explore differentially expressed lncRNAs in intrinsic tamoxifen-resistant and tamoxifen-sensitive BC tissue (Figure 1A). In total 2,262 lncRNAs demonstrated significantly greater expression in tamoxifen-resistant tissue (fold change > 2). The microarray was also used to explore differentially expressed lncRNAs between the tamoxifen-resistant BC cell line (MCF-7R) and parental cells (MCF-7) (Figure 1B), revealing that 706 lncRNAs demonstrated significantly greater expression in MCF-7R cells. Given that tissue- and cell-specific expression patterns are often driven by epigenomic changes, we performed an integrative analysis using these lncRNA microarray data and retrieved H3K27ac chromatin immunoprecipitation sequencing (ChIP-seq) data of MCF-7R and MCF-7 cells from the GEO dataset (GSE106695) to identify the epigenetically activated lncRNAs

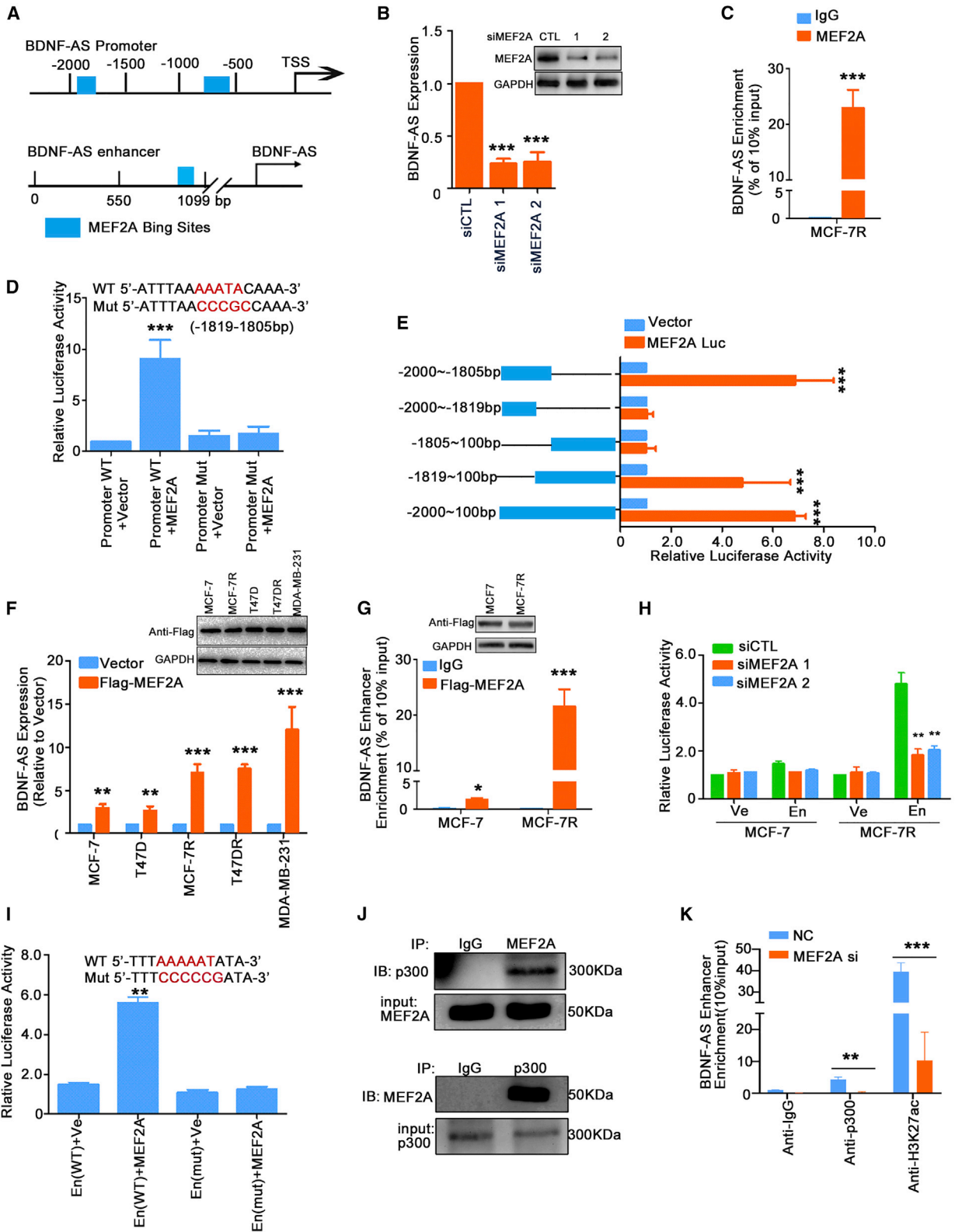
that were involved in endocrine resistance. Focusing on the non-coding genome, we found that 1,204 and 1,351 lncRNA loci had H3K27ac modification in MCF-7 and MCF-7R cells, respectively (Figures S1A and S1B). Among them, 269 lncRNAs had higher H3K27ac peak levels in MCF-7R than MCF-7 cells, suggesting that these lncRNAs may be epigenetically activated in MCF-7R cells (Figure 1C). We then intersected the expression change of lncRNAs with H3K27ac ChIP-seq data and noted that 8 lncRNAs were overexpressed with higher H3K27ac peaks in MCF-7R cells (Figure 1D), suggesting that the increased expression of these lncRNAs was driven by the histone acetylation of the corresponding *cis*-regulatory region. Among these lncRNAs, BDNF-AS exhibited the highest expression and the highest H3K27ac signals in MCF-7R compared with MCF-7 cells (Figures 1D and S1C). Meanwhile, BDNF-AS was among the top overexpressed lncRNAs in tamoxifen-resistant tissue compared with tamoxifen-sensitive tissue (Figure 1A).

BDNF-AS is a natural antisense lncRNA of brain-derived neurotrophic factor (BDNF) and is located at chr11:p14.1 (Modarresi et al., 2012). There were about 680 copies/cell of BDNF-AS transcript in MDA-MB-231, 385 copies/cell in MCF-7R cells, and 25 copies/cell in MCF-7 cells (Figure S1D). The H3K27ac peaks in the promoter of BDNF-AS were similar in MCF-7R and MCF-7 cells (Figure 1E). However, the H3K27ac signal was significantly higher in the region containing the 40 kb upstream of BDNF-AS in MCF-7R than that in MCF-7 cells (Figure 1E), suggesting that an enhancer located in that region (chr11:27485364-27486463) might have driven the overexpression of BDNF-AS.

Endocrine-resistant BC cells frequently acquire aggressive biological features that are similar to those of TNBC cells (Bui et al., 2017; Fu et al., 2017). Therefore, we also analyzed H3K27ac peaks of MDA-MB-231 cells from the GEO dataset (GSE85158) (Figure S1E) and found 3,438 overlapping H3K27ac peak sites between MCF-7R and MDA-MB-231 cells. Among these sites, 113 H3K27ac peaks were higher in MCF-7R than in MCF-7 cells, including the peak located around the

Figure 1. Epigenetically Activated BDNF-AS Is Associated with Endocrine Resistance of BC and Promotes Cancer Cell Proliferation

- (A) Microarray analysis of lncRNA expression in six cases of breast tumor tissue, including three intrinsic tamoxifen-resistant cases and three tamoxifen-sensitive cases. A heatmap was generated from the log-transformed and average normalized fluorescent intensity for each sample.
- (B) Microarray analysis of lncRNA expression in tamoxifen-resistant MCF-7 (MCF-7R) BC cells and parental tamoxifen-sensitive MCF-7 cells. A heatmap was generated from the log-transformed and average normalized fluorescent intensity for each sample.
- (C) H3K27ac modification in MCF-7 and MCF-7R cells detected using ChIP-seq in the GEO dataset (GSE106695). A heatmap was generated from the log-transformed and average normalized H3K27ac peak levels for each sample.
- (D) Correlation of H3K27ac signal and the expression of lncRNAs in MCF-7R normalized to MCF-7.
- (E) Gene tracks of H3K27Ac ChIP-seq occupancy at the *cis*-regulatory region of lncRNA BDNF-AS in MCF-7, MCF-7R, and MDA-MB 231. The x axis shows genomic position, and enhancer-containing regions are depicted in the box (En). A non-regulatory region (NC) nearby the enhancer was used as the negative control for the luciferase assay. The y axis shows the sequencing depth at this position.
- (F) ChIP-PCR assays detected H3K27ac at the enhancer region of BDNF-AS in parental and tamoxifen-resistant cells, as well as in MDA-MB-231. Bar graphs represent mean \pm SD of triplicate experiments. ***p < 0.001.
- (G and H) The luciferase assay demonstrated that the predicated enhancer-containing sequence enhanced the transcription activity in MCF-7R (G) and T47DR (H) cells but not in MCF-7 (G) and T47D (H) cells.
- (I) Deletion of the enhancer of BDNF-AS in MCF-7R restored BDNF-AS expression to the level of MCF-7.
- (J) ChIP assays detected H3K27ac at the enhancer region of BDNF-AS in BC tissue. Endocrine-sensitive luminal type, n = 10; endocrine-resistant luminal type, n = 12 (tamoxifen-resistant, n = 6; aromatase inhibitor-resistant, n = 6); triple-negative BC, n = 10. Bar graphs represent mean \pm SD. ***p < 0.001.
- (K) BDNF-AS levels in BC tissue, as detected using qRT-PCR.
- (L) BDNF-AS knockdown sensitized MCF-7 cells to tamoxifen treatment.
- (M) Knockdown of BDNF-AS restored the sensitivity of MCF-7R cells to tamoxifen.
- (N) Knockdown of BDNF-AS inhibited cell proliferation in MDA-MB-231 cells, as detected using MTT assays. The mean \pm SD is shown for three independent experiments in (L), (M), and (N). ***p < 0.001. See also Figure S1.



(legend on next page)

predicted BDNF-AS enhancer (Figure 1E). Confirmed by ChIP-PCR, H3K27ac was increasingly enriched at the predicted BDNF-AS enhancer locus in MCF-7R, T47DR (endocrine-resistant), and MDA-MB-231 than in MCF-7 and T47D cells (Figure 1F). Moreover, the luciferase vector containing the enhancer sequence could dramatically increase the transcription of BDNF-AS in MCF-7R and T47DR cells, but not in MCF-7 and T47D cells (Figures 1G and 1H). The expression of BDNF-AS in MCF-7R cells decreased to a level close to that of MCF-7 cells after deleting enhancer by Cas9 (Figure 1I). Furthermore, H3K27ac enrichment was higher in endocrine-resistant BC tissue and TNBC tissue compared with endocrine-sensitive BC tissue (Figure 1J). Also, expression of BDNF-AS in endocrine-resistant BC and TNBC tissue was higher than that in endocrine-sensitive BC tissue (Figure 1K), consistent with the results of cell lines (Figure S1F). These results suggest that high BDNF-AS expression is due to the epigenomic activation of the enhancer upstream of BDNF-AS in BC tissue and cells.

To further explore the role of BDNF-AS in endocrine resistance and proliferation of BC cells, we used plasmid-mediated overexpression or small interfering RNA (siRNA)-mediated knockdown to manipulate BDNF-AS expression in MCF-7, MCF-7R, MDA-MB-231, and T47DR cells (Figures S1G–S1J). MTT assays showed that the overexpression of BDNF-AS in MCF-7 cells promoted cell proliferation and enhanced resistance to tamoxifen treatment (Figure 1L). On the other hand, BDNF-AS knockdown significantly re-sensitized MCF-7R and T47DR cells to tamoxifen treatment (Figures 1M and S1K) and inhibited cell proliferation in MCF-7R, T47DR, and MDA-MB-231 cells (Figures 1M, 1N, and S1L). Similarly, enforced expression of BDNF-AS in MCF-7 could boost the number of colonies, even under tamoxifen treatment (Figure S1M). Moreover, knockdown of BDNF-AS significantly decreased colony formation in MCF-7R, T47DR, and MDA-MB-231 cells and re-sensitized MCF-7R and T47DR cells to tamoxifen treatment (Figures S1M–S1O). These results confirm the involvement of BDNF-AS in BC endocrine resistance and the proliferation of cancer cells.

MEF2A Binds to BDNF-AS Enhancer and Elevates Its Transcription

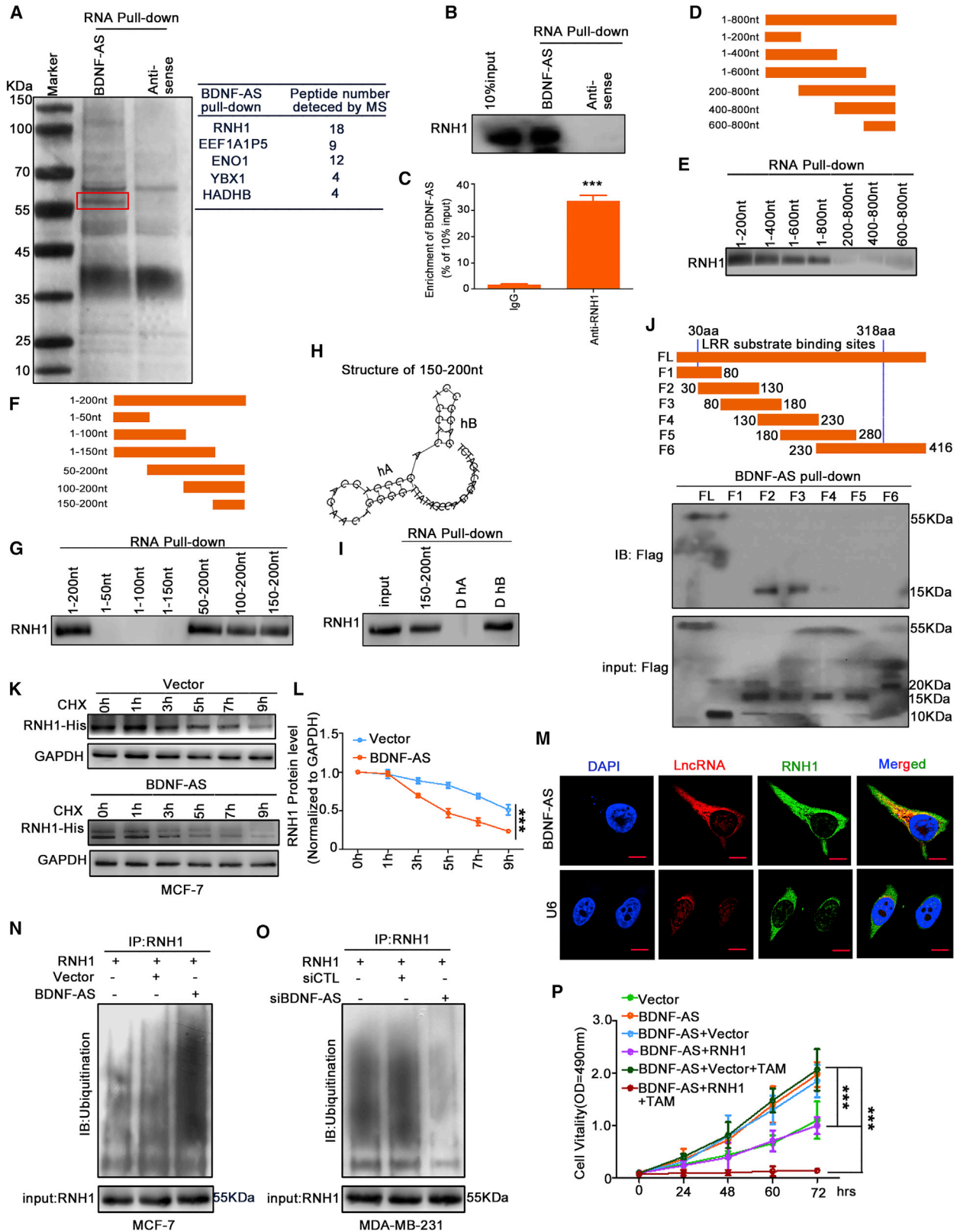
We have indicated that the overexpression of BDNF-AS was driven by epigenetically activated enhancers in endocrine-resistant BC cells and tissue. It is well established that transcription

factors coordinate epigenetic modification and subsequent transcription regulation (Calo and Wysocka, 2013). To identify the transcription factors responsible for activating BDNF-AS transcription, we analyzed the BDNF-AS promoter region (2.0 kb upstream of the transcription start site [TSS]) and the enhancer region (chr11:27485364–27486463) (JASPAR database). MEF2A had two potential binding sites in the promoter region and one binding site in the enhancer region of BDNF-AS (Figures 2A, S2A, and S2B). Thus, we investigated whether BDNF-AS was induced by MEF2A and found that the knockdown of MEF2A decreased BDNF-AS expression in MCF-7R cells (Figure 2B). The ChIP-PCR assay detected the binding of MEF2A to the promoter in MCF-7R (Figure 2C). Luciferase reporter assay was then used to examine the binding region of MEF2A with BDNF-AS promoter and revealed that the –1819 to –1805 bp site is essential for MEF2A-mediated transactivation (Figure 2D). Further mutations in the –1819 to –1805 bp site markedly decreased BDNF-AS transcription induced by MEF2A (Figure 2E).

As shown in Figure 1D, the H3K27ac peaks were similar among MCF-7, MCF-7R, and MDA-MB-231 cells in the promoter; the enforced expression of MEF2A indeed similarly enhanced the activity of BDNF-AS promoter among MCF-7, T47D, MCF-7R, T47DR, and MDA-MB-231 cells (Figure S2C). In addition, the enforced expression of MEF2A dramatically increased the expression of BDNF-AS in MCF-7R, T47DR, and MDA-MB-231 cells but only slightly increased BDNF-AS expression in MCF-7 and T47D cells (Figure 2F). This is consistent with the observation that MEF2A had dramatically higher binding affinity with BDNF-AS enhancer in MCF-7R, T47DR, and MDA-MB-231 cells compared with MCF-7 and T47D cells (Figures 2G and S2D), suggesting that MEF2A drove the BDNF-AS overexpression in MCF-7R, T47DR, and MDA-MB-231 cells via coordination with the BDNF-AS enhancer. This speculation was further confirmed by knockdown of MEF2A, which revealed that enhancer activity was dramatically decreased in MCF-7R cells but not in MCF-7 cells (Figure 2H). Additionally, the luciferase reporter assay confirmed that MEF2A could interact only with wild-type (WT) BDNF-AS enhancer, but not the mutant enhancer, to upregulate BDNF-AS transcription (Figure 2I). The MEF2 family functions as the scaffold protein to interact with histone acetylase p300 and co-activates the transcription of targeted gene (Ichihara et al., 2018). Immunoprecipitation (IP) assay showed that MEF2A interacted with p300 in MCF-7R cells

Figure 2. MEF2A Binds to BDNF-AS Enhancer and Elevates Its Transcription

- (A) Prediction of potential MEF2A-binding sites in BDNF-AS promoter or enhancer region by JASPAR. The predicted MEF2A binding sites are shown as blue boxes.
- (B) MEF2A knockdown decreased BDNF-AS expression.
- (C) ChIP assays show the binding of MEF2A to the promoter of region of BDNF-AS in MCF-7R cells. IgG was used as the negative control.
- (D) Luciferase activity showed that MEF2A binds to the –1819 to –1805 bp site of the promoter region of BDNF-AS.
- (E) Mutation of the –1819 to –1805 bp site abolished luciferase activity.
- (F) Enforced expression of MEF2A increased BDNF-AS expression.
- (G) ChIP assays showed the binding of MEF2A to the enhancer of region of BDNF-AS in MCF-7 and MCF-7R cells.
- (H) Knockdown of MEF2A decreased enhancer activity in MCF-7R cells.
- (I) Mutation of the MEF2A binding site abolished MEF2A-mediated enhancer activity in luciferase assay.
- (J) MEF2A acted as the scaffold protein for p300. MEF2A antibody or p300 antibody was used to immunoprecipitate p300 or MEF2A in MCF-7R cells. Immunoblotting detected both MEF2A and p300. IgG was the negative control.
- (K) Silencing MEF2A decreased the enrichment of both p300 and H3K27ac with BDNF-AS.
- All bar graphs represent mean \pm SD of triple independent experiments. * $p < 0.05$, ** $p < 0.01$, and *** $p < 0.001$. See also Figure S2.



(legend on next page)

(Figure 2J). When silencing MEF2A in MCF-7R cells, the enrichment of p300 and H3K27ac in the enhancer region of BDNF-AS was markedly decreased (Figure 2K). These results revealed that MEF2A was the co-activator that coordinated with p300 in the enhancer to enhance transcription of BDNF-AS.

BDNF-AS Induces Endocrine Resistance by Interacting with Ribonuclease Inhibitor 1 to Promote Its Ubiquitin-Mediated Degradation

It is well established that the majority of lncRNAs exert their functions by interacting with their counterpart proteins (Guttman and Rinn, 2012). Ribonuclease inhibitor 1 (RNH1) was identified to be a BDNF-AS binding protein (Figure 3A). RNH1 has been reported to be localized mainly in the cytoplasm (Haigis et al., 2003), with a similar subcellular distribution as BDNF-AS (Figures S3A–S3C). We confirmed the interaction of BDNF-AS with RNH1 using RNA pull-down assay followed by western blotting (Figure 3B) and RNA IP (RIP) in MDA-MB-231 cells (Figure 3C). Notably, BDNF-AS was enriched by about 30-fold in the precipitates with RNH1 antibodies (Figure 3C). RNA pull-down assay demonstrated that BDNF-AS mutants containing nucleotides 150–200 retained the capability to bind to RNH1 as efficiently as the full-length BDNF-AS (Figures 3D–3G, S3D, and S3E). Furthermore, two hairpin structures within nucleotides 150–200 were predicted by RNAfold, which we named hairpin A (hA) and hairpin B (hB) (Figure 3H). Deleting hA (D hA) failed to bind to RNH1. However, deletion of the hB could not abolish the interaction between BDNF-AS and RNH1 (Figure 3I). Additionally, IP of RNH1 also specifically retrieved BDNF-AS fragment (nucleotides 1–200) (Figure S3F). On the other hand, the binding motif of RNH1 to BDNF-AS was determined and revealed that BDNF-AS bond the 80–130 amino acid (aa) region of RNH1 (Figure 3J). Then, co-location of BDNF-AS and RNH1 in cytoplasm was detected by immunofluorescence assay followed by fluorescence *in situ* hybridization (FISH) assay (Figure 3M). These data suggest that BDNF-AS interacts with RNH1 in cytoplasm.

RNH1 has been reported to be a tumor suppressor in melanoma, gastric cancer, and bladder cancer (Li et al., 2014; Peng et al., 2014; Yao et al., 2013), although its function and regulatory

mechanism has not been clearly demonstrated. To explore how RNH1 was regulated by BDNF-AS, we found that the protein level of RNH1 decreased upon BDNF-AS overexpression (Figure S3G). Consistently, BDNF-AS knockdown increased the protein level of RNH1 (Figure S3I), while RNH1 mRNA was not affected upon either BDNF-AS overexpression or knockdown (Figures S3H and S3J). Next, through the cycloheximide (CHX) chase assay, we found that the enforced expression of BDNF-AS resulted in faster degradation of RNH1 in MCF-7 cells (Figures 3K and 3L). On the other hand, the half-life of RNH1 protein was prolonged when the expression of BDNF-AS was silenced in MDA-MB-231 cells (Figures S3K and S3L).

Ubiquitination is the most common mechanism that regulates protein degradation. We used UbiBrowser (<http://ubibrowser.ncpsb.org>) and found that RNH1 was a potential substrate of various E3 ligases (Figure S3M). We then performed an *in cellulo* ubiquitination assay and found a significant increase in polyubiquitinated RNH1 protein in cells that overexpressed BDNF-AS (Figure 3N), whereas knocking down BDNF-AS decreased RNH1 ubiquitination (Figure 3O). Collectively, BDNF-AS regulated RNH1 protein degradation through ubiquitination.

The MTT assays and colony formation showed that ectopically expressed RNH1 could almost abolish BDNF-AS-mediated effects on BC proliferation and resistance to tamoxifen (Figure 3P; Figure S3N). Together, these results revealed that BDNF-AS interacted with RNH1 in the cytoplasm and functioned as an oncogenic lncRNA via the promotion of RNH1 ubiquitin-mediated degradation.

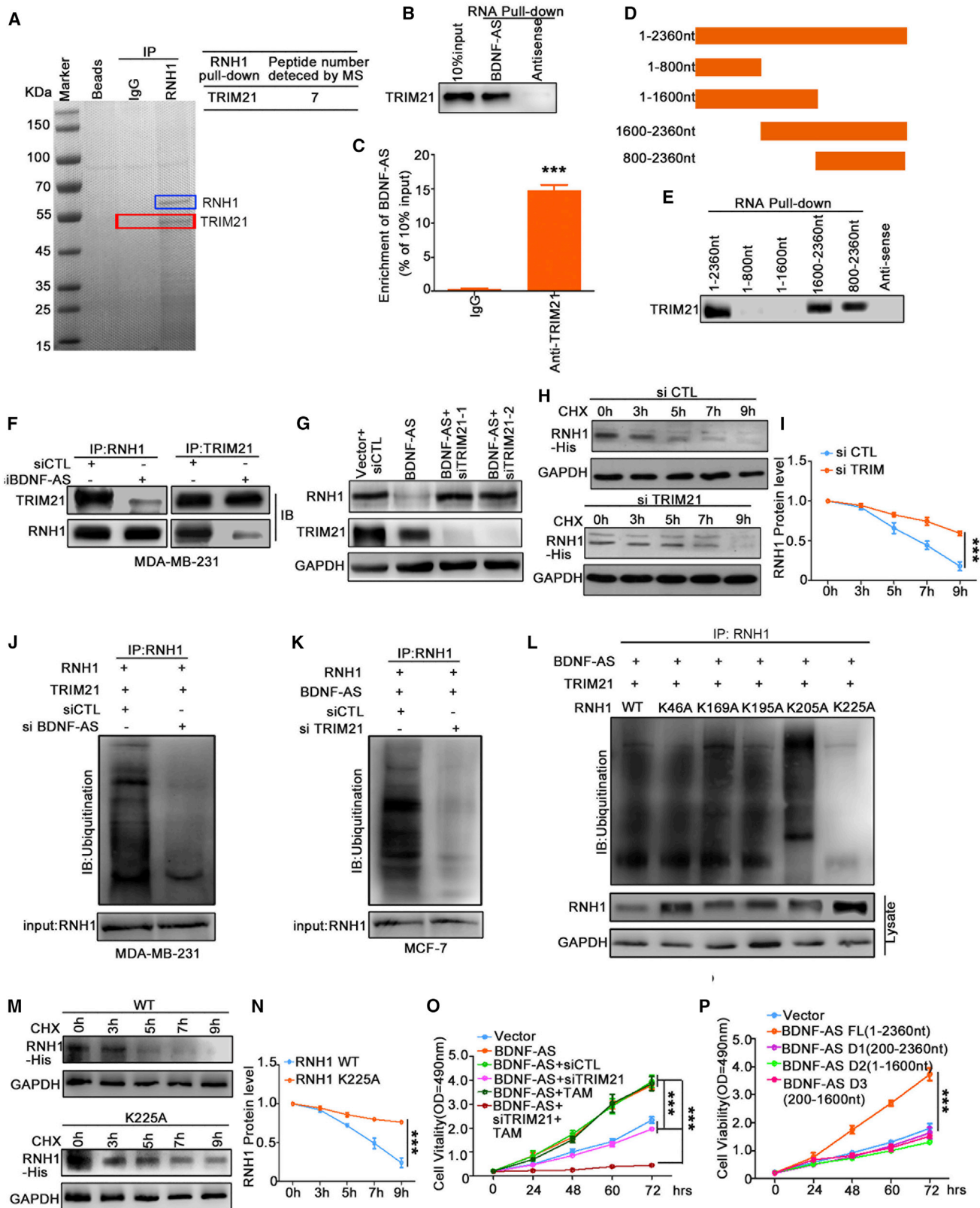
BDNF-AS Recruits TRIM21 to Degrade RNH1 via Ubiquitination

lncRNAs can act as guides, decoys, or scaffolds to participate in signal transduction. Therefore, we hypothesized that BDNF-AS functioned as the scaffold to recruit an E3 ligase to RNH1 and promote RNH1 degradation. TRIM21, an E3 ligase that has been reported to be involved in innate immune diseases (Pan et al., 2016) was identified as a candidate BDNF-AS-binding E3 ligase that mediated the ubiquitination of RNH1 (Figure 4A). RNA pull-down also showed the interaction of BDNF-AS with TRIM21

Figure 3. BDNF-AS Interacts with RNH1 to Induce RNH1 Degradation, Leading to Endocrine Resistance and Proliferation of Cancer Cells

- (A) RNA pull-down of BDNF-AS followed by mass spectrometry identification. The bands in frames, which were specifically precipitated by BDNF-AS, but not by antisense RNA, were submitted for mass spectrometric detection.
- (B) BDNF-AS pull-down followed by western blot exhibited the binding of BDNF-AS to RNH1. The antisense of BDNF-AS was used as the negative control.
- (C) RIP assay showed the binding of BDNF-AS to RNH1.
- (D–G) RNA pull-down via sequential truncated BDNF-AS fragments showed the binding region of BDNF-AS with RNH1. (D and E) Nucleotide 1–200 fragment, which contained the binding motif of BDNF-AS with RNH1. (F and G) Nucleotide 150–200 fragment, which contained the binding motif of BDNF-AS with RNH1.
- (H) The structure of BDNF-AS fragment (nucleotides 150–200) predicted by RNAfold. There were two hairpin loops (hA and hB) in this fragment.
- (I) The deletion of hairpin A (D hA) but not hairpin B abolished the binding of BDNF-AS fragment (nucleotides 150–200) with RNH1.
- (J) The 80–130 aa region of RNH1 protein harbored a domain for the binding of BDNF-AS.
- (K and L). Overexpression of BDNF-AS promoted RNH1 degradation. Immunoblotting detection of His tag is shown as mean \pm SD of three independent experiments in (K). *** $p < 0.001$.
- (M) BDNF-AS co-located with RNH1 in cytoplasm. The co-location of RNH1 (green) and BDNF-AS (red) was detected using immunofluorescence followed by fluorescence *in situ* hybridization assay. U6, which located mainly in nucleus, was used as control. Scale bars, 50 μ m.
- (N and O). BDNF-AS promoted RNH1 ubiquitination and degradation, as detected using *in cellulo* ubiquitination assays in MCF-7 cells (N) and MDA-MB-231 cells (O).
- (P) RNH1 abrogated BDNF-AS-promoted cell proliferation and tamoxifen resistance. Error bars indicate mean \pm SD of triple independent experiments. *** $p < 0.001$.

See also Figure S3.



(legend on next page)

(Figure 4B). RIP followed by qRT-PCR confirmed that BDNF-AS was markedly enriched in the precipitate of TRIM21 antibody (Figure 4C). Moreover, LacZ and IncNKILA were used as negative control to confirm the specific binding between BDNF-AS and RNH1/TRIM21 (Figure S4A). BDNF-AS fragments containing nucleotides 1600–2360 bound to TRIM21 as efficiently as the full-length BDNF-AS, whereas other fragments completely lost their binding capacity, suggesting that nucleotides 1600–2360 of BDNF-AS harbored the domain that interacted with TRIM21 (Figures 4D and 4E). Additionally, IP of TRIM21 specifically retrieved BDNF-AS nucleotides 1600–2360 (Figure S4B). These results suggest that BDNF-AS serves as a scaffold to recruit TRIM21 to RNH1.

Next, we found that BDNF-AS siRNAs decreased the interaction of RNH1 with TRIM21 markedly, while the enforced expression of BDNF-AS increased the interaction of RNH1 with TRIM21 (Figure 4F; Figure S4C). To validate whether TRIM21 mediated RNH1 degradation, we detected the RNH1 protein level after TRIM21 RNAi. We found that siTRIM21 drastically decreased BDNF-AS-dependent RNH1 degradation (Figure 4G) and prolonged the half-life of RNH1 in the degradation assay (Figures 4H and 4I). In addition, RNH1 ubiquitination was dramatically reduced upon either siBDNF-AS or siTRIM21 silencing (Figures 4J and 4K). These results support the suggestion that TRIM21 is the E3 ligase that regulates RNH1 ubiquitination.

To identify the lysine site(s) of RNH1 for ubiquitination, UbPred (<http://www.ubpred.org>) was used for prediction. Five lysine sites were predicted as candidates with the most potential for ubiquitination. We substituted each of these five lysine residues with alanine in RNH1 and performed ubiquitination assay in BDNF-AS and TRIM21-overexpressing cells (Figure 4L). In contrast to WT and other mutants, K225A mutant largely abolished the ubiquitination of RNH1 (Figure 4L). Consistently, when the K225A mutant was subjected to the protein half-life assay, it was significantly more stable than WT RNH1 (Figures 4M and 4N), and its half-life was similar to that of WT RNH1 in the TRIM21 knockdown cells (Figure 4H). Together, these results demonstrated that BDNF-AS fostered the interaction of RNH1 with TRIM21, thus promoting TRIM21-mediated ubiquitination on K225 of RNH1 to induce degradation of RNH1.

We further found that TRIM21 RNAi abolished BDNF-AS-induced tamoxifen resistance in MCF-7 cells (Figures 4O and S4D). On the other hand, the BDNF-AS fragments without the binding region to RNH1 (BDNF-AS D1) or the binding region to TRIM21 (BDNF-AS D2) as well as the fragment deleting both of the regions (BDNF-AS D3) did not promote BC cell proliferation and colony formation (Figures 4P and S4E). These data support the finding that the function of BDNF-AS relies on its binding with both RNH1 and TRIM21.

BDNF-AS Activated mTOR Signaling via Abolishing RNH1-Mediated mTOR mRNA Decay

RNH1 was reported to suppress PI3K/AKT/mTOR signaling and subsequent exertion of its anti-tumor effects in bladder cancer (Peng et al., 2014). However, the mechanism of how PI3K/AKT/mTOR signaling was inactivated by RNH1 is not clear yet. Here, we found that the mTOR level as well as the activity of downstream signaling, including pS6K and p4EBP1 (downstream of mTORC1) and pAKT (S473) (downstream of mTORC2), decreased upon siBDNF-AS and showed recovery after knocking down RNH1 (Figure 5A). Consistently, overexpression of BDNF-AS increased mTOR levels, while the enforced expression of RNH1 abolished the BDNF-AS-mediated activation of mTOR-related signaling (Figure S5A). These data suggest that the BDNF-AS/RNH1 axis upregulates the mTOR level to activate its downstream signaling of both mTORC1 and mTORC2.

Furthermore, we found that RNH1 knockdown resulted in an increased level of mTOR mRNA (Figure 5B), which was decreased by exogenous expression of RNH1 (Figure S5B). Interestingly, the stability of endogenous mTOR mRNA improved upon RNH1 knockdown (Figure 5C), whereas enforced expression of RNH1 promoted the decay of endogenous mTOR mRNA (Figure S5C). However, RNH1 did not affect the exogenous mTOR transcript without the 3' UTR (Figures S5D and S5E). RNH1 has been reported to bind to the components of RNA-induced silencing complex (RISC), such as poly(A) binding protein Pab1 (PABPC1) (Chennupati et al., 2018; Moretti et al., 2012), we speculated that RNH1 mediated the decay of mTOR mRNA via a microRNA (miRNA)-dependent mechanism.

Figure 4. BDNF-AS Links TRIM21 with RNH1 to Promote RNH1 Ubiquitinated Degradation

- (A) TRIM21 was identified as a RNH1-binding protein using mass spectrometry. The bands that were specifically precipitated by RNH1, but not by IgG or beads, were submitted for mass spectrometric detection.
- (B) BDNF-AS pull-down followed by immunoblotting exhibited the binding of BDNF-AS to TRIM21.
- (C) RIP assay showed the binding of BDNF-AS to TRIM21.
- (D and E) RNA pull-down using sequential truncated BDNF-AS fragments (D) showed that nucleotides 1600–2360 of BDNF-AS contains the binding motif with TRIM21 (E).
- (F) Silencing BDNF-AS decreased the interaction of RNH1 with TRIM21.
- (G) Knockdown of TRIM21 abrogated the BDNF-AS-mediated degradation of RNH1 protein.
- (H and I) Silencing of TRIM21 prolonged the degradation of RNH1. Immunoblotting detection of His tag is shown in (H).
- (J) Knockdown of BDNF-AS decreased the ubiquitination of RNH1.
- (K) Knockdown of TRIM21 decreased the ubiquitination of RNH1. The bottom panels depict the input of the cell lysates.
- (L) Mutation of K225A abolished the ubiquitination of RNH1. RNH1 was mutated at five putative ubiquitination residues. Wild-type or mutant RNH1 was transfected into HeLa cells for 12 h and then transfected with BDNF-AS and TRIM21 plasmids for another 24 h. MG132 (20 nM) was added 5 h before harvesting.
- (M and N) K225A mutation of TRIM21 could not mediate RNH1 degradation (M). Band intensity was quantified using ImageJ software (N).
- (O) Silencing TRIM21 abrogated BDNF-AS-promoted cell proliferation and tamoxifen resistance.
- (P) The full length is essential for BDNF-AS to promote cell proliferation. Sequentially deleted BDNF-AS fragments were constructed and transfected into MCF-7 cells. FL, full length of BDNF-AS; D1, the mutant deleting nucleotides 1–200 that contained RNH1 binding site; D2, the mutant deleting nucleotides 1600–2360 that contained TRIM21 binding site; D3, the mutant deleting both nucleotides 1–200 and nucleotides 1600–2360.
- Error bars indicate mean \pm SD of three independent experiments. *** p < 0.001. See also Figure S4.

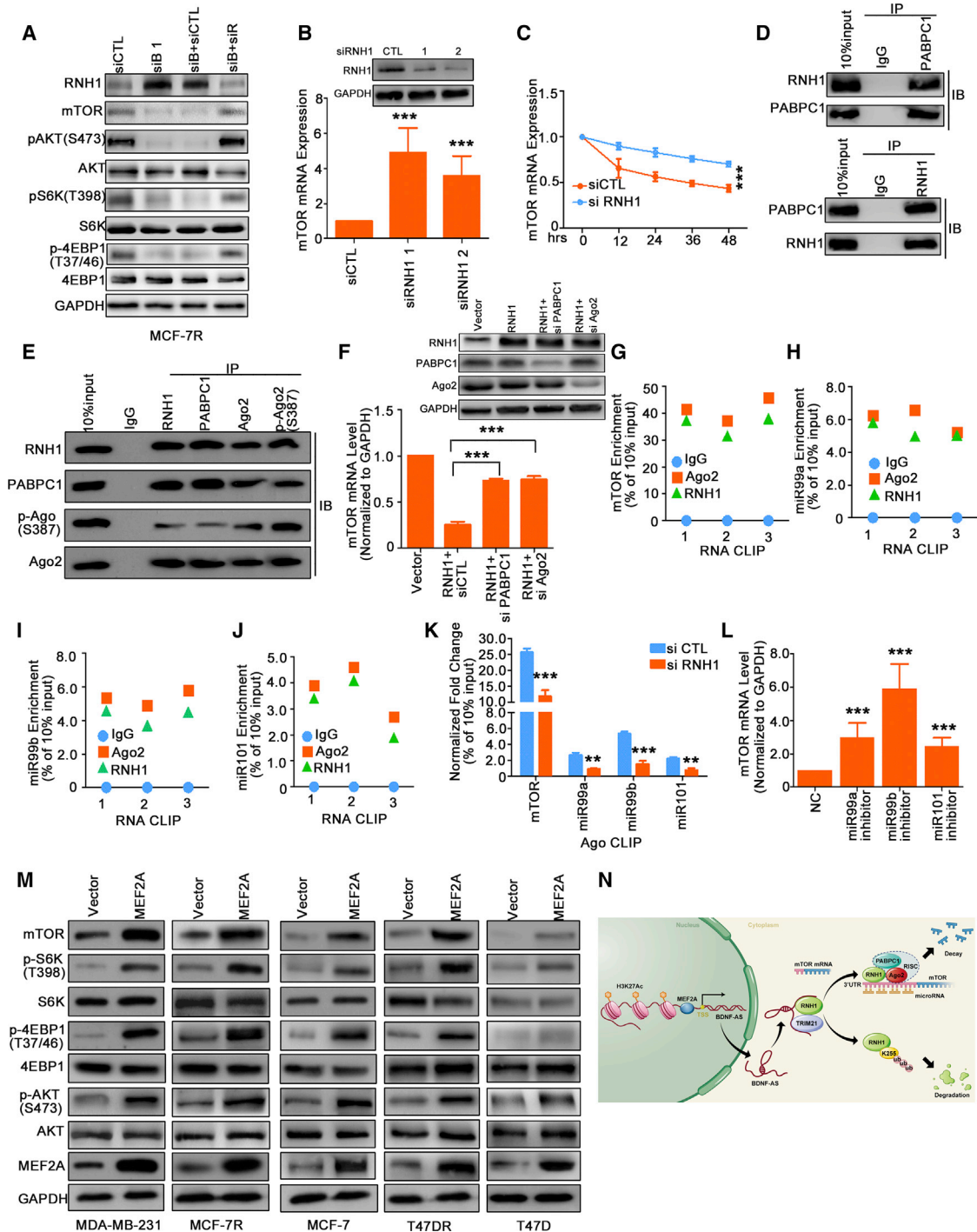


Figure 5. RNH1 Facilitates RNA-Induced Suppressed Complex (RISC) to Accelerate the mRNA Decay of mTOR

(A) Knockdown of BDNF-AS decreased mTOR levels and its downstream signaling activity in MCF-7R cells.
 (B) qRT-PCR detection of mTOR mRNA level in RNH1 silencing MCF-7 cells.
 (C) RNH1 promoted mTOR mRNA decay. qRT-PCR detected mTOR mRNA levels at each time point.
 (D) Co-immunoprecipitation showed the binding of RNH1 to PABPC1.
 (E) Co-immunoprecipitation showed the binding of RNH1 to the active RISC.
 (F) Silencing PABPC1 or Ago2 reversed RNH1-promoted mTOR mRNA decay.
 (G) RNH1 and Ago2 bound to mTOR mRNA, as detected by CLIP. Results are shown as individual enrichment for each independent experiment.

(legend continued on next page)

Through co-IP assay, we confirmed the binding of RNH1 with both PABPC1 (Figure 5D) and phosphorylated Ago2 (Figure 5E). Furthermore, we found that RNH1-mediated downregulation of mTOR mRNA level was rescued by RNAi of either PABPC1 or Ago2 (Figure 5F), suggesting that RNH1 promoted mTOR mRNA decay through the RISC-mediated silencing mechanism. This was further confirmed by RNA cross-linking IP (CLIP) assays, which showed that endogenous mTOR mRNA could be precipitated with the RNH1-associated RISC (Figure 5G), while exogenous mTOR mRNA that lacked the 3' UTR could rarely be precipitated with RNH1-associated RISC (Figure S5F).

A set of miRNAs, including miR-99a, miR-99b, and miR-101, have been shown to target mTOR in various tumors (Gui and Shen, 2012; Sun et al., 2011; Zhang et al., 2017). RNA CLIP assays verified that miR-99a, miR-99b, and miR-101 were specifically precipitated with both RNH1 and Ago2, indicating that they were loaded into RISC for mTOR mRNA decay (Figures 5H–5J). In line with this result, RNH1 knockdown reduced the binding between mTOR mRNA, miR-99a, miR-99b, and miR-101 and RISC (Figure 5K). Consistently, inhibitors of miR-99a, miR-99b, and miR-101 led to upregulation of the mRNA levels of mTOR (Figure 5L). We found no significant change of the other target genes (SNF2H, FGFR3, HOXA1, SMARCA5, IGF1R, RB1, TET2, EZH2, and FZD4) of miR-99a, miR-99b, and miR-101, as demonstrated in other studies (Mueller et al., 2013; Wang et al., 2017; Wu et al., 2020; Chen et al., 2019; Lin et al., 2017; Hisaoka et al., 2011; Jing et al., 2018; Chen et al., 2020; Du et al., 2018), when knocking down RNH1 (Figure S5K). On the other hand, a few of the other miRNAs that did not target at mTOR, including miR-24, miR-200, and miR-203a, did not participate in the RNH1-mediated RISC silencing mechanism of mTOR mRNA (Figures S5G–S5I). Knocking down RNH1 exerted no effect on the binding between miR-24, miR-200, and miR-203a and RISC (Figure S5J). In summary, our data reveal a mechanism whereby RNH1 interacts with RISC and recruits a set of miRNAs to degrade mTOR mRNA, which in turn reduces mTOR downstream signaling.

We have shown that the enrichment of MEF2A to the enhancer of BDNF-AS was much higher in MDA-MB-231, MCF-7R, and T47DR cells than in that in MCF-7 and T47D cells and thus mediated overexpression of BDNF-AS in MDA-MB-231, MCF-7R, and T47DR cells (Figures 2F and 2G; Figure S2D). Consistently the enforced expression of MEF2A increased the levels of mTOR and its downstream signaling in MDA-MB-231, MCF-7R, and T47DR cells to a much higher degree compared with that in MCF-7 and T47D cells (Figure 5M). These results suggest that MEF2A mediates the transcriptional activation of BDNF-AS via coordination with the enhancer, and then the overexpressed BDNF-AS activates the RNH1/TRIM21/mTOR cascade (Figure 5N).

Characterization of BDNF-AS as a Biomarker for Endocrine Resistance and Progression of BC

In 162 cases of BC tissue, including 100 cases of TNBC and 62 cases of luminal BC (32 cases of intrinsic endocrine-resistant and 30 cases of endocrine-sensitive), both BDNF-AS and mTOR expression were significantly lower in the endocrine-sensitive breast tissues compared with the TNBC and endocrine-resistant cancer tissues, whereas RNH1 expression showed the opposite staining trend (Figures 6A–6D). BDNF-AS expression was negatively correlated with RNH1 and positively correlated with mTOR levels in both our BC cohorts and TCGA dataset (Figures 6E, 6F and S6A–S6C) and was prone to be positive correlation in endocrine-resistant BC (Figure S6D). Concordantly, RNH1 expression was negatively correlated with mTOR in BC (Figure 6G). Moreover, high levels of BDNF-AS in BC tissue were significantly associated with higher histopathological grading, larger tumor size, lymph node, and distant metastasis, as well as advanced disease staging (Table S1). Notably, overexpression of BDNF-AS featured endocrine resistance (Figure 6H). High BDNF-AS expression was associated with poor overall survival and disease-free survival in both our BC cohorts and The Cancer Genome Atlas (TCGA) dataset (Figures 6I–6L and S6E–S6K). In addition, BDNF-AS was an independent prognostic predictor for poor survival of BC patients, which was even stronger than lymph node and distant metastasis (Figure 6M; Table S2). Consistently, higher RNH1 expression was associated with better overall survival (Figure 6N), whereas intensive mTOR expression was associated with poor overall survival in our cohort (Figure 6O). These data suggest that the BDNF-AS level serves as a predictive marker for poor outcome and endocrine resistance of BCs.

Targeting mTOR Overcomes BDNF-AS-Induced Endocrine Resistance in BC Xenografts

MCF-7 has a PIK3CA E545K mutation, and T47D has a PIK3CA H1047R mutation, both of which render the activation of the PI3K pathway (Bachman et al., 2004). The PI3K inhibitor alpelisib only slightly inhibited MCF-7R and T47DR cell growth, even when combined with tamoxifen (Figures S7A and S7B). However, the mTOR inhibitor everolimus significantly suppressed cell proliferation, especially when combined with tamoxifen (Figures S7A and S7B), which suggests that mTOR inhibition could restore endocrine sensitivity to these tamoxifen-resistant cells.

To further demonstrate the role of overexpression of BDNF-AS in the induction of endocrine resistance, MCF-7 cells with doxycycline (DOX)-inducible BDNF-AS were implanted into the fat pads of nude mice (Figure S7C). The tumors with overexpression of BDNF-AS grew at a much faster rate than the vector control group and became resistant to tamoxifen

(H–J) RNH1 and Ago2 bound to miR-99a (H), miR-99b (I), and miR-101 (J) which specifically targeted mTOR mRNA. Results were shown as individual enrichment for each independent experiment.

(K) Silencing of RNH1 decreased the binding of Ago2 to mTOR mRNA or to indicated miRNAs.

(L) mTOR mRNA was upregulated after inhibition of miRNAs.

(M) Enforced expression of MEF2A activated the mTOR signaling pathway.

(N) The schematic working model of BDNF-AS overexpression drives mTOR signaling. The enhancer-driven overexpression of BDNF-AS promoted RNH1 protein degradation via TRIM21-mediated ubiquitination. Thus BDNF-AS abolished RNH1-regulated and RISC-mediated mTOR mRNA decay, which led to prolonged mTOR mRNA stability.

All bar graphs represent mean \pm SD of triplicate experiments. * $p < 0.05$, ** $p < 0.01$, and *** $p < 0.001$. See also Figure S5.

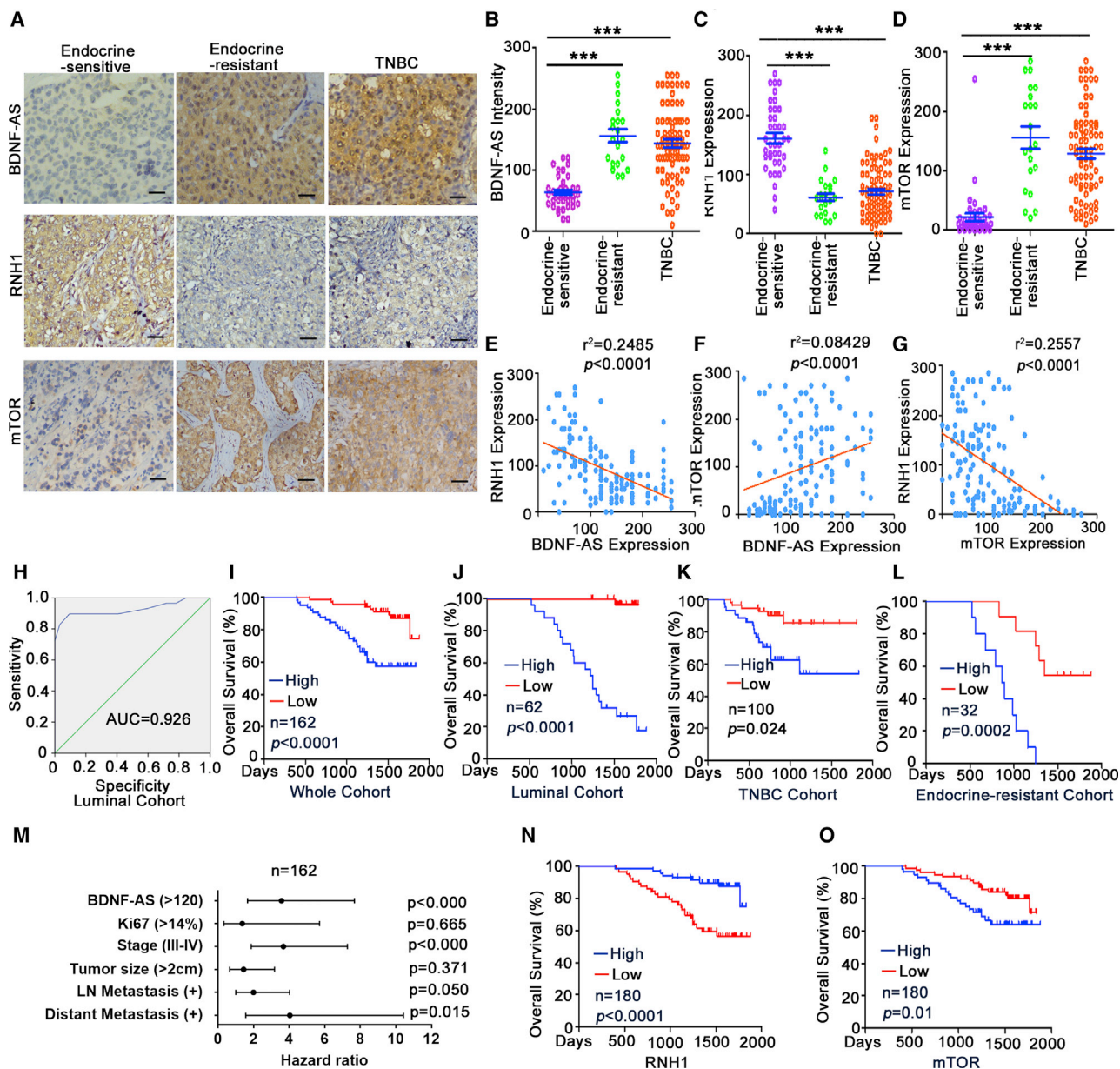


Figure 6. BDNF-AS as a Biomarker to Predict Endocrine Resistance and Poor Prognosis of BC Patients

(A) Representative images showing ISH of BDNF-AS and IHC of RNH1 and mTOR. Scale bars, 50 μ m.

(B–D) Expression of BDNF-AS (B), RNH1 (C), and mTOR (D) in BC tissues, detected by ISH (BDNF-AS) and IHC (RNH1, mTOR). The signal of ISH and IHC was quantified using ImageJ. *** $p < 0.001$.

(E–G) A scatter diagram showing the negative correlation between BDNF-AS and RNH1 (E), the positive correlation between BDNF-AS and mTOR (F), and the negative correlation between RNH1 and mTOR (G).

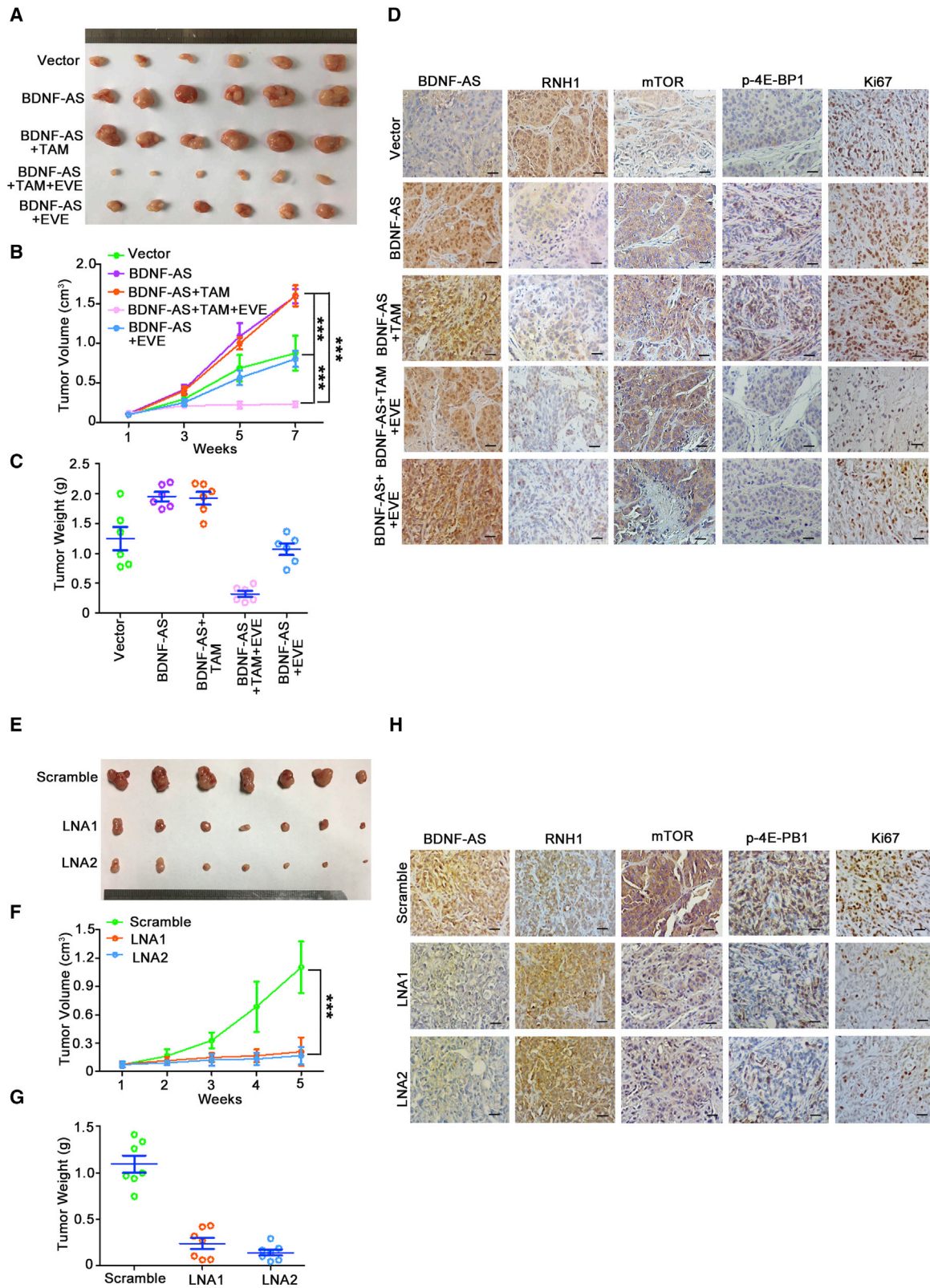
(H) Receiver-operating characteristic (ROC) curve shows the value of BDNF-AS for distinguishing endocrine-resistant from endocrine-sensitive HR-positive BCs.

(I–L) High levels of BDNF-AS were correlated with poor overall survival of BC patients. Kaplan-Meier survival of BC patients with a median follow-up period of 2,000 days was analyzed in all cases (I), luminal cancers (J), TNBC (K), and endocrine-resistant cancers, including tamoxifen-resistant ($n = 17$) and aromatase inhibitor-resistant ($n = 15$) (L).

(M) Multivariate Cox proportional-hazard analysis of prognostic variables in 162 cases of BC patients.

(N and O) Low levels of RNH1 (N) and high levels of mTOR (O) were correlated with poor overall survival of BC patients. Kaplan-Meier survival of BC patients with a median follow-up period of 2,000 days was analyzed in all cases.

See also [Figure S6](#) and [Tables S1](#) and [S2](#).



(legend on next page)

treatment. In contrast, the combination of tamoxifen with everolimus considerably reduced tumor growth and restored sensitivity to endocrine therapy in BDNF-AS-overexpression tumors (Figures 7A–7C). Again, the corresponding expression of the BDNF-AS/RNH1/mTOR cascade was confirmed in the xenograft by *in situ* hybridization (ISH) and immunohistochemistry (IHC) (Figure 7D), and Ki67 staining indicated cell proliferation in these tumors (Figure 7D).

We then used locked nucleic acid (LNA)-based antisense oligonucleotides to evaluate the *in vivo* therapeutic effects of targeting BDNF-AS (Figure S7D). The BDNF-AS-targeting LNAs significantly decreased tumor growth compared with the control LNA treatment (Figures 7E–7G). ISH and IHC were used to confirm the corresponding changes of BDNF-AS/RNH1/mTOR cascade in the xenograft tissue (Figure 7H). Consistently, Ki67 staining was relatively low in the BDNF-AS LNA treatment groups (Figure 7H). Collectively, these data suggest that mTOR inhibitor could be applied to overcome BDNF-AS-induced endocrine resistance. Targeting BDNF-AS may serve as a promising strategy to reverse endocrine therapy resistance as well as to prevent BC progression.

DISCUSSION

Aberrations in the PI3K/AKT/mTOR pathway have been implicated in the development of many cancers and resistance to cancer therapies (Vivanco and Sawyers, 2002). Specifically for BCs, multiple therapeutic strategies have been developed to target various components of this pathway to prevent cancer progression, as well as to reverse endocrine resistance. The mechanism of how the PI3K/AKT/mTOR pathway is activated varies among different cases of BCs, such as amplification of HER2, mutation of PI3K/AKT, and loss of PTEN (Arpino et al., 2009; Riggins et al., 2007). Herein, we discovered a mechanism whereby the enhancer-driven overexpression of BDNF-AS activated mTOR signaling in endocrine-resistant BCs and TNBCs by promoting degradation of RNH1 protein, and we identified MEF2A as the transcription factor that interacted with both BDNF-AS enhancer and promoter, which specifically drove the overexpression of BDNF-AS. As the function of lncRNA depends on cell type and subcellular location, BDNF-AS could also be located in the nucleus in cervical cancer and esophageal cancer and function as a tumor suppressor by participating in epigenetic regulation of target genes (Zhang et al., 2018; Zhao et al., 2018). Above all, our results suggest that BDNF-AS acts as an oncogene in endocrine-resistant BCs as well as in TNBCs.

RNH1 acts as a tumor suppressor in several types of cancers (Li et al., 2014; Peng et al., 2014; Yao et al., 2013). However, its

function and regulatory mechanism remain poorly understood. Our data reveal that RNH1 interacts with RISC and is involved in mTOR mRNA degradation, adding another layer of regulation of mTOR activity at the mRNA level. Moreover, we elucidated the regulatory mechanism of RNH1 by demonstrating that TRIM21 is the E3 ligase that mediates RNH1 degradation via the induction of ubiquitination on K225 of RNH1. Recent studies show that targeted degradation is a new frontier for therapeutics, and molecular glues act like adhesives, bringing the E3s and targeted protein together (Baek and Schulman, 2020). Our data support the suggestion that BDNF-AS works as a molecular glue to bind TRIM21 to RNH1 and induce RNH1 degradation.

Clinically, BDNF-AS is a strong independent prognostic predictor of poor survival and is correlated with endocrine resistance of HR-positive BCs. Our data suggest that the BDNF-AS/RNH1/TRIM21/mTOR cascade could directly activate mTOR signaling despite the status of PI3K. Monitoring the BDNF-AS level raises the possibility of precision prediction of endocrine resistance in HR-positive BC patients, which indicates that further application of mTOR inhibitors or targeting of BDNF-AS is needed to re-sensitize the tumor to endocrine therapy or to prevent BC progression, even in PIK3CA-mutated cancer.

STAR★METHODS

Detailed methods are provided in the online version of this paper and include the following:

- KEY RESOURCES TABLE
- RESOURCE AVAILABILITY
 - Lead Contact
 - Materials Availability
 - Data and Code Availability
- EXPERIMENTAL MODEL AND SUBJECT DETAILS
 - Patients tissue specimens
 - Cells and cell culture
 - Animals
- METHOD DETAILS
 - siRNA /shRNA, sgDNA and constructs
 - Quantitative RT-PCR
 - Microarray
 - Identification of H3K27ac ChIP-sequence
 - Colony formation assay
 - MTS cell viability assay
 - Tissue samples, ISH, immunohistochemical staining (IHC), and fluorescence *in situ* hybridization (FISH)
 - Western blot analysis
 - Chromatin immunoprecipitation assays

Figure 7. BDNF-AS as a Potential Therapeutic Target for BC Progression and Endocrine Resistance

(A–C) Enforced expression of BDNF-AS increased tumor growth and induced tamoxifen resistance of breast tumors in nude mice. The harvested tumors are shown in (A). Growth curves (B) and tumor weights (C) are mean \pm SD of six mice in each group. *** $p < 0.001$.

(D) Expression of BDNF-AS/RNH1/mTOR cascade and Ki67 in MCF-7 xenograft tissues. BDNF-AS expression was detected using ISH, and the expression of RNH1, mTOR, p-4E-BP1, and Ki67 was detected using IHC. Scale bars, 50 μ m.

(E–G) Knockdown of BDNF-AS reduced the tumor burden in nude mice. The harvested tumors are shown in (E). Growth curves (F) and tumor weights (G) are mean \pm SD of seven mice in each group. *** $p < 0.001$.

(H) Expression of BDNF-AS/RNH1/mTOR cascade and Ki67 in MDA-MB-231 xenograft tissues. Scale bars, 50 μ m.

See also Figure S7.

- RNA immunoprecipitation (RIP)
- RNA pulldown assay
- Cycloheximide (CHX) chase measurements of RNHI half-life
- mRNA decay measurements
- Immunoprecipitation (IP) and ubiquitination assay
- Luciferase reporter assay
- RNA-CLIP
- Animal experiments

● **QUANTIFICATION AND STATISTICAL ANALYSIS**

SUPPLEMENTAL INFORMATION

Supplemental Information can be found online at <https://doi.org/10.1016/j.celrep.2020.107753>.

ACKNOWLEDGMENTS

This work was supported by grants from the National Science and Technology Major Project (2020ZX09201021), the National Key Research and Development Program of China (2016YFC1302301), the Natural Science Foundation of China (81672738, 81730077, and U1601223), the Guangzhou Science, Technology and Innovation Commission (201704020095 and 201704020131), a program from the Guangdong Basic and Applied Basic Research Foundation (2019A1515110082), a program from Guangdong Introducing Innovative and Entrepreneurial Teams (2016ZT06S252 and 2016ZT06S638), and grants from Natural Science Foundation of Guangdong Province (2017A030313828).

AUTHOR CONTRIBUTIONS

Conceptualization, H.H. and H.Y.; Methodology, H.H., H.Y., X.L., X.D., and Qingjian Li.; Investigation, H.H., H.Y., X.L., S.C., X.D., Qingjian Li., W.C., C.W., Q.H., F.Z., S.Z., D.-C.L., Y.Y., X.X., and Z.X.; Data Analysis, H.H., H.Y., X.L., X.D., and D.-C.L.; Resources, H.H., H.Y., X.L., Z.X., Z.W., and Qiang Liu.; Writing, H.H., D.-C.L., and X.L.

DECLARATION OF INTERESTS

The authors declare no competing interests.

Received: November 26, 2019

Revised: April 20, 2020

Accepted: May 19, 2020

Published: June 9, 2020

REFERENCES

AlFakeeh, A., and Brezden-Masley, C. (2018). Overcoming endocrine resistance in hormone receptor-positive breast cancer. *Curr. Oncol.* *25* (Suppl 1), S18–S27.

Amin, V., Harris, R.A., Onuchic, V., Jackson, A.R., Charnecki, T., Paithankar, S., Lakshmi Subramanian, S., Riehle, K., Coarfa, C., and Milosavljevic, A. (2015). Epigenomic footprints across 111 reference epigenomes reveal tissue-specific epigenetic regulation of lincRNAs. *Nat. Commun.* *6*, 6370.

Arpino, G., De Angelis, C., Giuliano, M., Giordano, A., Falato, C., De Laurentiis, M., and De Placido, S. (2009). Molecular mechanism and clinical implications of endocrine therapy resistance in breast cancer. *Oncology* *77* (Suppl 1), 23–37.

Bachman, K.E., Argani, P., Samuels, Y., Silliman, N., Ptak, J., Szabo, S., Konishi, H., Karakas, B., Blair, B.G., Lin, C., et al. (2004). The PIK3CA gene is mutated with high frequency in human breast cancers. *Cancer Biol. Ther.* *3*, 772–775.

Baek, K., and Schulman, B.A. (2020). Molecular glue concept solidifies. *Nat. Chem. Biol.* *16*, 2–3.

Bui, Q.T., Im, J.H., Jeong, S.B., Kim, Y.M., Lim, S.C., Kim, B., and Kang, K.W. (2017). Essential role of Notch4/STAT3 signaling in epithelial-mesenchymal transition of tamoxifen-resistant human breast cancer. *Cancer Lett.* *390*, 115–125.

Calo, E., and Wysocka, J. (2013). Modification of enhancer chromatin: what, how, and why? *Mol. Cell* *49*, 825–837.

Campos-Parra, A.D., López-Urrutia, E., Orozco Moreno, L.T., López-Camarillo, C., Meza-Menchaca, T., Figueroa González, G., Bustamante Montes, L.P., and Pérez-Plasencia, C. (2018). Long non-coding RNAs as new master regulators of resistance to systemic treatments in breast cancer. *Int. J. Mol. Sci.* *19*, E2711.

Cedar, H., and Bergman, Y. (2009). Linking DNA methylation and histone modification: patterns and paradigms. *Nat. Rev. Genet.* *10*, 295–304.

Chen, H., Lin, F., Xing, K., and He, X. (2015). The reverse evolution from multicellularity to unicellularity during carcinogenesis. *Nat. Commun.* *6*, 6367.

Chen, L., Long, Y., Han, Z., Yuan, Z., Liu, W., Yang, F., Li, T., Shu, L., and Zhong, Y. (2019). MicroRNA-101 inhibits cell migration and invasion in bladder cancer via targeting FZD4. *Exp. Ther. Med.* *17*, 1476–1485.

Chen, Q., Li, X., Kong, L., Xu, Q., Wang, Z., and Lv, Q. (2020). miR-101-3p induces vascular endothelial cell dysfunction by targeting tet methylcytosine dioxygenase 2. *Acta Biochim. Biophys. Sin. (Shanghai)* *52*, 180–191.

Chennupati, V., Veiga, D.F., Maslowski, K.M., Andina, N., Tardivel, A., Yu, E.C., Stilianovic, M., Simillion, C., Duchosal, M.A., Quadroni, M., et al. (2018). Ribonuclease inhibitor 1 regulates erythropoiesis by controlling GATA1 translation. *J. Clin. Invest.* *128*, 1597–1614.

Cristofanilli, M., Turner, N.C., Bondarenko, I., Ro, J., Im, S.A., Masuda, N., Coleoni, M., DeMichele, A., Loi, S., Verma, S., et al. (2016). Fulvestrant plus palbociclib versus fulvestrant plus placebo for treatment of hormone-receptor-positive, HER2-negative metastatic breast cancer that progressed on previous endocrine therapy (PALOMA-3): final analysis of the multicentre, double-blind, phase 3 randomised controlled trial. *Lancet Oncol.* *17*, 425–439.

Dowsett, M., Forbes, J.F., Bradley, R., Ingle, J.N., Aihara, T., Bliss, J.M., Boccardo, F., Coates, A.S., Coombes, R.C., and Cuzick, J.; Early Breast Cancer Trialists' Collaborative Group (EBCTCG) (2015). Aromatase inhibitors versus tamoxifen in early breast cancer: patient-level meta-analysis of the randomised trials. *Lancet* *386*, 1341–1352.

Du, X., Qi, F., Lu, S., Li, Y., and Han, W. (2018). Nicotine upregulates FGFR3 and RB1 expression and promotes non-small cell lung cancer cell proliferation and epithelial-to-mesenchymal transition via downregulation of miR-99b and miR-192. *Biomed. Pharmacother.* *101*, 656–662.

Du, Z., Fei, T., Verhaak, R.G., Su, Z., Zhang, Y., Brown, M., Chen, Y., and Liu, X.S. (2013). Integrative genomic analyses reveal clinically relevant long non-coding RNAs in human cancer. *Nat. Struct. Mol. Biol.* *20*, 908–913.

Finn, R.S., Martin, M., Rugo, H.S., Jones, S., Im, S.A., Gelmon, K., Harbeck, N., Lipatov, O.N., Walshe, J.M., Moulder, S., et al. (2016). Palbociclib and letrozole in advanced breast cancer. *N. Engl. J. Med.* *375*, 1925–1936.

Fu, H., Fu, L., Xie, C., Zuo, W.S., Liu, Y.S., Zheng, M.Z., and Yu, J.M. (2017). miR-375 inhibits cancer stem cell phenotype and tamoxifen resistance by degrading HOXB3 in human ER-positive breast cancer. *Oncol. Rep.* *37*, 1093–1099.

Gui, T., and Shen, K. (2012). miRNA-101: a potential target for tumor therapy. *Cancer Epidemiol.* *36*, 537–540.

Guttman, M., and Rinn, J.L. (2012). Modular regulatory principles of large non-coding RNAs. *Nature* *482*, 339–346.

Guttman, M., Amit, I., Garber, M., French, C., Lin, M.F., Feldser, D., Huarte, M., Zuk, O., Carey, B.W., Cassady, J.P., et al. (2009). Chromatin signature reveals over a thousand highly conserved large non-coding RNAs in mammals. *Nature* *458*, 223–227.

Haigis, M.C., Kurten, E.L., and Raines, R.T. (2003). Ribonuclease inhibitor as an intracellular sentry. *Nucleic Acids Res.* *31*, 1024–1032.

- Hisaoka, M., Matsuyama, A., Nagao, Y., Luan, L., Kuroda, T., Akiyama, H., Kondo, S., and Hashimoto, H. (2011). Identification of altered MicroRNA expression patterns in synovial sarcoma. *Genes Chromosomes Cancer* *50*, 137–145.
- Ichihara, M., Kamiya, T., Hara, H., and Adachi, T. (2018). The MEF2A and MEF2D function as scaffold proteins that interact with HDAC1 or p300 in SOD3 expression in THP-1 cells. *Free Radic. Res.* *52*, 799–807.
- Iyer, M.K., Niknafs, Y.S., Malik, R., Singhal, U., Sahu, A., Hosono, Y., Barrette, T.R., Prensner, J.R., Evans, J.R., Zhao, S., et al. (2015). The landscape of long noncoding RNAs in the human transcriptome. *Nat. Genet.* *47*, 199–208.
- Jing, P., Zhao, N., Ye, M., Zhang, Y., Zhang, Z., Sun, J., Wang, Z., Zhang, J., and Gu, Z. (2018). Protein arginine methyltransferase 5 promotes lung cancer metastasis via the epigenetic regulation of miR-99 family/FGFR3 signaling. *Cancer Lett.* *427*, 38–48.
- Kolch, W., Halasz, M., Granovskaya, M., and Kholodenko, B.N. (2015). The dynamic control of signal transduction networks in cancer cells. *Nat. Rev. Cancer* *15*, 515–527.
- Li, L., Pan, X.Y., Shu, J., Jiang, R., Zhou, Y.J., and Chen, J.X. (2014). Ribonuclease inhibitor up-regulation inhibits the growth and induces apoptosis in murine melanoma cells through repression of angiogenin and ILK/PI3K/AKT signaling pathway. *Biochimie* *103*, 89–100.
- Lin, Y., Deng, W., Pang, J., Kemper, T., Hu, J., Yin, J., Zhang, J., and Lu, M. (2017). The microRNA-99 family modulates hepatitis B virus replication by promoting IGF-1R/PI3K/Akt/mTOR/ULK1 signaling-induced autophagy. *Cell. Microbiol.* *19* (5).
- Martin, C., and Zhang, Y. (2005). The diverse functions of histone lysine methylation. *Nat. Rev. Mol. Cell Biol.* *6*, 838–849.
- Modarresi, F., Faghihi, M.A., Lopez-Toledano, M.A., Fatemi, R.P., Magistri, M., Brothers, S.P., van der Brug, M.P., and Wahlestedt, C. (2012). Inhibition of natural antisense transcripts in vivo results in gene-specific transcriptional upregulation. *Nat. Biotechnol.* *30*, 453–459.
- Moretti, F., Kaiser, C., Zdanowicz-Specht, A., and Hentze, M.W. (2012). PABP and the poly(A) tail augment microRNA repression by facilitated miRISC binding. *Nat. Struct. Mol. Biol.* *19*, 603–608.
- Mueller, A.C., Sun, D., and Dutta, A. (2013). The miR-99 family regulates the DNA damage response through its target SNF2H. *Oncogene* *32*, 1164–1172.
- Murakawa, Y., Yoshihara, M., Kawaji, H., Nishikawa, M., Zayed, H., Suzuki, H., and Hayashizaki, Y.; Fantom Consortium (2016). Enhanced identification of transcriptional enhancers provides mechanistic insights into diseases. *Trends Genet.* *32*, 76–88.
- Pan, J.A., Sun, Y., Jiang, Y.P., Bott, A.J., Jaber, N., Dou, Z., Yang, B., Chen, J.S., Catanzaro, J.M., Du, C., et al. (2016). TRIM21 ubiquitylates SQSTM1/p62 and suppresses protein sequestration to regulate redox homeostasis. *Mol. Cell* *62*, 149–151.
- Peng, Y., Li, L., Huang, M., Duan, C., Zhang, L., and Chen, J. (2014). Angiogenin interacts with ribonuclease inhibitor regulating PI3K/AKT/mTOR signaling pathway in bladder cancer cells. *Cell. Signal.* *26*, 2782–2792.
- Riggins, R.B., Schrecengost, R.S., Guerrero, M.S., and Bouton, A.H. (2007). Pathways to tamoxifen resistance. *Cancer Lett.* *256*, 1–24.
- Sun, D., Lee, Y.S., Malhotra, A., Kim, H.K., Matecic, M., Evans, C., Jensen, R.V., Moskaluk, C.A., and Dutta, A. (2011). miR-99 family of microRNAs suppresses the expression of prostate-specific antigen and prostate cancer cell proliferation. *Cancer Res.* *71*, 1313–1324.
- Vivanco, L., and Sawyers, C.L. (2002). The phosphatidylinositol 3-Kinase AKT pathway in human cancer. *Nat. Rev. Cancer* *2*, 489–501.
- Wang, J.-G., Tang, W.-P., Liao, M.-C., Liu, Y.-P., and Ai, X.-H. (2017). HOXA1-MiR-99a suppresses cell invasion and metastasis in nasopharyngeal carcinoma through targeting. *Oncotargets Ther.* *10*, 753–761.
- Wu, K., Jiang, Y., Zhou, W., Zhang, B., Li, Y., Xie, F., Zhang, J., Wang, X., Yan, M., Xu, Q., et al. (2020). Long noncoding RNA RC3H2 facilitates cell proliferation and invasion by targeting microRNA-101-3p/EZH2 axis in OSCC. *Mol. Ther. Nucleic Acids* *20*, 97–110.
- Wu, S.C., Kallin, E.M., and Zhang, Y. (2010). Role of H3K27 methylation in the regulation of lncRNA expression. *Cell Res.* *20*, 1109–1116.
- Yao, X., Li, D., Xiong, D.M., Li, L., Jiang, R., and Chen, J.X. (2013). A novel role of ribonuclease inhibitor in regulation of epithelial-to-mesenchymal transition and ILK signaling pathway in bladder cancer cells. *Cell Tissue Res.* *353*, 409–423.
- Zhang, Y., Huang, B., Wang, H.Y., Chang, A., and Zheng, X.F.S. (2017). Emerging role of microRNAs in mTOR signaling. *Cell. Mol. Life Sci.* *74*, 2613–2625.
- Zhang, H., Liu, C., Yan, T., Wang, J., and Liang, W. (2018). Long noncoding RNA BDNF-AS is downregulated in cervical cancer and has anti-cancer functions by negatively associating with BDNF. *Arch. Biochem. Biophys.* *646*, 113–119.
- Zhao, H., Diao, C., Wang, X., Xie, Y., Liu, Y., Gao, X., Han, J., and Li, S. (2018). LncRNA BDNF-AS inhibits proliferation, migration, invasion and EMT in oesophageal cancer cells by targeting miR-214. *J. Cell. Mol. Med.* *22*, 3729–3739.

STAR★METHODS

KEY RESOURCES TABLE

REAGENT or RESOURCE	SOURCE	IDENTIFIER
Antibodies		
mTOR (7C10) Rabbit mAb	Cell Signaling Technology	2983S;RRID:AB_2105622
Akt Antibody	Cell Signaling Technology	9272;RRID:AB_329827
Phospho-Akt (Ser473) Antibody	Cell Signaling Technology	9271;RRID:AB_329825
p70 S6 Kinase Antibody	Cell Signaling Technology	9202;RRID:AB_331676
Phospho-Drosophila p70 S6 Kinase (Thr398) Antibody	Cell Signaling Technology	9209;RRID:AB_2269804
4E-BP1 Antibody	Cell Signaling Technology	9452;RRID:AB_331692
Phospho-4E-BP1 (Thr37/46) Antibody	Cell Signaling Technology	9459;RRID:AB_330985
TRIM21 (D1O1D) Rabbit mAb	Cell Signaling Technology	92043;RRID:AB_2800177
Ubiquitin Antibody	Cell Signaling Technology	3933;RRID:AB_2180538
Rabbit (DA1E) mAb IgG XP® Isotype Control	Cell Signaling Technology	3900;RRID:AB_1550038
Anti-Ribonuclease inhibitor antibody	Abcam	ab245627
Anti-MEF2A antibody	Abcam	Ab86755;RRID:AB_10674453
Anti-Agonaute 2 antibody	Abcam	Ab32381;RRID:AB_867543
Anti-Argonaute-2 (phospho S387) antibody	Abcam	Ab215744
Anti-digoxigenin AP-conjugate	Roche	11093274910;RRID:AB_514497
PABPC1 antibody	Proteintech	10970-1-AP;RRID:AB_10596918
HRP-conjugated GAPDH Antibody	Proteintech	HRP-60004;RRID:AB_2737588
Anti-acetyl-Histone H3 (Lys27) Antibody	Millipore	07-360;RRID:AB_310550
Anti-Flag M2 antibody	Sigma	F3165;RRID:AB_259529
Bacterial and Virus Strains		
E.coli DH5 α Electro-Cells	TAKARA	9027
Biological Samples		
Breast tumor tissues	Shantou Affiliated Hospital, Sun Yat-sen University	N/A
Chemicals, Peptides, and Recombinant Proteins		
Actinomycin	Sigma-Aldrich	SBR00013
Cycloheximide	Sigma-Aldrich	239763-M
MG132	Sigma-Aldrich	M7449
Alpelisib	Selleck	S2814
4-Hydroxytamoxifen	Sigma-Aldrich	H6278
Doxycycline	Sigma-Aldrich	D9891
17 β -ESTRADIOL(pellets)	Innovative Research of America	E-121
TAMOXIFEN (FREE BASE)(pellets)	Innovative Research of America	E-361
Everolimus	Selleck	S1120
Critical Commercial Assays		
Agilent Human lncRNA Microarray V6	Agilent technologies	74348
Deposited Data		
lncRNA microarray data	This paper	MendeleyData https://data.mendeley.com/datasets/mssgvrt7rh/draft?a=b2927384-88c8-43f4-9e1c-8e43ce1102cd
Experimental Models: Cell Lines		
MDA-MB-231	ATCC	HTB-26
MCF-7	ATCC	HTB-22

(Continued on next page)

Continued

REAGENT or RESOURCE	SOURCE	IDENTIFIER
T47D	ATCC	HTB-133
HEK-293T	ATCC	CRL-3216
MCF-7R	This paper	N/A
T47DR	This paper	N/A
HELA	ATCC	CCL-2
Experimental Models: Organisms/Strains		
Mouse: CAnN.Cg-Foxn1nu/Crl(BALB/c Nude)	Charles River	SCXK 2016-0006
Oligonucleotides		
Primers for QRT-PCR, see Table S3	Generay	www.generay.com.cn/
BDNF-AS si 1: 5'-GGCTCACCAGTTGTTTGT-3'	Thermofisher	www.thermofisher.com
BDNF-AS si 2: 5'-GCTAATCTTACAACAGCAC-3'	Thermofisher	www.thermofisher.com
RNH1 si 1: 5'-TACGACATTTACTGGTCTGAGGA GATGGA-3'	Thermofisher	www.thermofisher.com
RNH1 si 2: 5'-TGCTCTGGTTGGCCGACTGCGAT GTGAGT-3'	Thermofisher	www.thermofisher.com
TRIM21 si 1: 5'-TGAGAAGTTGGAAGTGAAAT-3'	Thermofisher	www.thermofisher.com
TRIM21 si 2: 5'-TGGAAGTGAAATTGCAATAA-3'	Thermofisher	www.thermofisher.com
MEF2A si 1: 5'-CACATTCTGCTGAATTATTA-3'	Thermofisher	www.thermofisher.com
MEF2A si 2: 5'-AAGTAATTATTAGGAATATAA-3'	Thermofisher	www.thermofisher.com
BDNF-AS probe: 5' Dig-AGTAGAGTTGACAGAG GAGTAT-Dig 3'	QIAGEN	https://www.qiagen.com/
sgRNA1: AGCTGTACTAGGCATAGCTA	Generay	www.generay.com.cn/
sgRNA2: CACACAAGTTGAAGTGACG	Generay	www.generay.com.cn/
LNA1: 5'-ATCGAGTCATCGCTGT-3'	QIAGEN	https://www.qiagen.com/
LNA2: 5'-CGAACACGTGATAGAA-3'	QIAGEN	https://www.qiagen.com/
See Table S3		N/A
Recombinant DNA		
pLVX-TETONE-Puro (TetOn)	Clontech	631849
pcDNA3.1/HisA	Invitrogen	V385-20
pGL3-Promoter	Promega	E1761
pGL3-Enhancer	Promega	E1771
Software and Algorithms		
SPSS 20.0	IBM	https://www.ibm.com/products/spss-statistics
ImageJ	NIH	http://imagej.net/
GraphPad Prism 8.0	GraphPad Software	https://www.graphpad.com/
Adobe Photoshop CS6	Adobe Design	www.photoshop.com

RESOURCE AVAILABILITY

Lead Contact

Further information and requests for resources and reagents should be directed to and will be fulfilled by the Lead Contact, Hai Hu (huhai@mail.sysu.edu.cn). This study did not generate new unique reagents.

Materials Availability

The plasmids and LNAs used in this study is available from the Lead Contact, Hai Hu (huhai@mail.sysu.edu.cn), upon completion of a materials transfer agreement.

Data and Code Availability

The accession number for the lncRNA microarray data in this paper is Mendeley Data <https://data.mendeley.com/datasets/mssgvr7rh/draft?a=b2927384-88c8-43f4-9e1c-8e43ce1102cd>

EXPERIMENTAL MODEL AND SUBJECT DETAILS

Patients tissue specimens

BC samples were obtained from female patients at the Breast Tumor Center, where 250 female BC (BC) samples were collected at Shantou Hospital of Sun Yat-sen University (Shantou, Guangdong, China) from 2009 to 2015. Pathological diagnosis was confirmed by two pathologists independently. All samples were collected with informed consents according to the International Ethical Guidelines for Biomedical Research Involving Human Subjects (CIOMS). Written informed consents were obtained from all patients before recruitment. All procedures performed in this study were in accordance with the ethical standards of the institutional research committee and the 1964 Helsinki Declaration and its later amendments or comparable ethical standards.

Cells and cell culture

MCF-7, T47D and MDA-MB-231 cells that were obtained from American Type Culture Collection (ATCC) were cultured in DMEM with 10% FBS and grown according to standard protocols. The establishment of tamoxifen-resistant cells (MCF-7R and T47DR) was previously described and culture was supplemented with 10% charcoal-stripped FBS (cFBS) (HyClone, USA) and 1 μ M 4-hydroxytamoxifen (Sigma-Aldrich, MO, USA).

Animals

All animal experiments were approved by Medical Ethics Committee of Sun Yat-sen University, following the Guidelines of Animal Handling and Care in Medical Research from Hunan Province, China. Animals were 4–6 weeks old female BALB/c nude mice, immune deficiency. All animals were drug or test naive and not involved in previous procedures. Mice were housed in a room with circulating air purification system in filter top, sawdust bedding cages. Cage was changed every 3 days in a laminar flow hood. Mice were feeded with sterile water and nude mice specific fodder.

METHOD DETAILS

siRNA /shRNA, sgDNA and constructs

Two siRNA/shRNA duplexes were used as listed in [Key Resources Table](#). The control siRNA/shRNA sequence is as follows: 5'-UAAGGCUAUGAAGAGAUAC-3'. The plko-tet-on "all-in-one" plasmid was used to generate the inducible expression of shBDNF-AS and shcontrol. BDNF-AS (Full length and mutants), RNH1, TRIM21, mTOR and MEF2A in pCDNA3.1 plasmid as well as Luciferase reporters were used for ectopic expression in cell lines. Lipofectamine 3000 (Invitrogen) was used for the siRNA or pCDNA3.1 plasmid transfection. Sequences of sgRNA for the knockout of BDNF-AS enhancer are:

sgRNA1, AGCTGTACTAGGCATAGCTA;
sgRNA2, CACACAAGTTGAAGTGTACG.

Quantitative RT-PCR

Total RNA was extracted from cultured cells according to standard protocols. 1 μ g of total RNA was reverse-transcribed into cDNAs using Superscript First-Strand cDNA Synthesis Kit (18080-051, Invitrogen, Carlsbad, CA). Quantitative RT-PCR was performed using SYBR Premix Ex TaqII kit (RRR081A, TAKARA, Otsu, Shiga, Japan) on LightCycler 480 System (Roche, Basel, Switzerland). The primers used for

Quantitative RT-PCR were listed in [Table S3](#).

Microarray

Microarray analysis was performed with labeled cDNA hybridized to Agilent Human lncRNA Microarray V6 (4*180K), a NimbleGen Hybridization System according to the manufacturer's protocol. After hybridization and washing, the processed pictures were scanned with the Agilent Microarray Scanner.

Identification of H3K27ac ChIP-sequence

The BC-related H3K27Ac histone modification ChIP-Seq datasets of Gene Expression Omnibus (GEO) database (MCF-7: GSM3096500, GSM3096501 and GSM3096502 with corresponding input: GSM3096509, GSM3096510 and GSM3096511; MCF-7R: GSM3096458, GSM3096459, GSM3096460 and with corresponding input GSM3096467, GSM3096468, GSM3096469; MDA-MB-231: GSM2258848, GSM2258849 and with corresponding input GSM2258864, GSM2258865) were used. The sratool-kit.2.9.2 tool was used to convert the sra format to the corresponding Fastq format followed by aligning Fastq files to the reference human genome assembly hg19 using Bowtie Aligner with defaults, except allowing only unique alignment. Bam files were subjected to identify peaks-enriched regions using the MACS1.4.2 (<http://liulab.dfci.harvard.edu/MACS/>) tool by considering reads mapped only once at a given locus. And then, cis-elements were identified using ROSE (<https://bitbucket.org/youngcomputation/rose>), where

closely spaced peaks within a 12.5 kb region were merged together and the signal strength of each cis-element was calculated by comparing H3K27Ac signal and input of the cis-element. Finally, cis-elements were assigned to the proximal ensemble genes using ROSE_geneMapper.py.

Colony formation assay

One thousand cells were plated in 6-well plates and cultured for 10 days. The colonies were stained with 1% crystal violet after fixation with 4% formaldehyde for 15 minutes.

MTS cell viability assay

One thousand cells were seeded into each well in 96-well plates. At each time point, cells were stained with sterile MTS mix liquid (1:10 in culture median) for 2 hours at 37°C in the dark. The absorbance was measured at 490 nm.

Tissue samples, ISH, immunohistochemical staining (IHC), and fluorescence *in situ* hybridization (FISH)

LncRNA BDNF-AS expression was measured in paraffin embedded samples using an ISH optimization kit (Roche, Basel, Switzerland) according to the manufacturer's instructions. The digoxigenin-labeled oligonucleotide probe targeting BDNF-AS (5' Dig-AGTAGAGTTGACAGAGGAGTAT-Dig 3') was designed and synthesized at Exiqon (Vedbaek, Denmark). Briefly, BC samples were treated with pepsin for 10 minutes at room temperature and incubated with 500 nM of probes at 55°C for 4 hours. The samples were incubated with blocking solution for 30 minutes, and secondary anti-digoxigenin (anti-DIG) antibody was applied for overnight. The HRP anti-AP reagent was used for 30 minutes after briefly washing in PBST. The diaminobenzidine was applied for coloration by interacting with HRP, and then hematoxylin was used for nucleus staining.

Immunohistochemistry (IHC) was performed according to the standard protocol. Primary antibodies were used (1:20-1:50) as listed in [Key Resources Table](#). The quantification of protein levels was evaluated by two independent pathologists. Both sets of results were combined to give a mean score for further comparative evaluations.

The ISH and IHC results were evaluated by two individuals in a blinded fashion; the evaluators scored the samples using a quick scoring system from 0 to 12 by combining the intensity and percentage of the positive signal (signal: "0," no staining; "1," weak staining; "2," intermediate staining; and "3," strong staining; percentage: "0," 0%; "1," 1%–25%; "2," 26%–50%; "3," 51%–75%; and "4," > 75%), and this was in good agreement with the initial quantification. An optimal cutoff value was identified. If the evaluated BDNF-AS score was higher than the average score, the BDNF-AS expression in those BC samples was classified as high; otherwise, it was classified as low. To account for inconsistencies in the percentage of the ISH signals, ImageJ software (National Institutes of Health, Bethesda, MD) was used for scoring signals. The data were statistically analyzed using the t test to determine the differences in BDNF-AS expression levels between different groups of tissues. $p < 0.05$ was considered statistically significant.

For FISH, cells were briefly rinsed in PBS and fixed in 4% formaldehyde in PBS (pH 7.4) for 40 minutes at room temperature. Then the cells were digested with 10% trypsin for 3 minutes at room temperature and permeabilized in PBS containing 0.1% Triton X-100 for 3 minutes at room temperature; washed with PBS three times for 10 minutes and washed with 75% ethanol at 4°C, 75% ethanol at –20°C, 85% ethanol at –20°C, and absolute ethanol at –20°C for 5 minutes. Then the cells were incubated with hybridization solution for 2 hours at 50°C prior to hybridization. Using the probe targeting BDNF-AS (5' Dig-AGTAGAGTTGACAGAGGAGTAT-Dig 3'), hybridization was performed in hybridization solution (probe dilution 1:1000, final concentration at 25 nm, Boster, China) for 16 hours at 50°C in a moist chamber. After hybridization, cells were washed in $2 \times$ SSC for 5 minutes at 50°C, and then in 50% deionized formamide / $4 \times$ SSC at 50°C for 25 minutes. For confocal microscopy, incubation of fluorescence-conjugated antibodies against DIG (Roche) was carried out overnight at 4°C. Hoechst33342 was then used for counterstaining the nuclei and images were obtained by laser scanning confocal microscopy (A1, Nikon).

Western blot analysis

Cells were lysed in RIPA lysis buffer (Beyotime, China) supplemented with protease and phosphatase inhibitors (Life Technologies, USA). Protein samples were subjected to 8% SDS-PAGE and transferred to PVDF membranes (Bio-Rad, USA). Membranes were then blocked with 5% non-fat milk in 0.1% TBST buffer overnight at 4°C. The membranes were subsequently incubated with antibodies (1:500-1:1000). The protein-antibody complex was detected using HRP-conjugated secondary antibodies and enhanced chemiluminescence (Pierce). The band intensity was quantified using ImageJ software (NIH, Bethesda).

Chromatin immunoprecipitation assays

Chromatin immunoprecipitation (ChIP) assays were performed using EZ-CHIP KIT according to the manufacturer's instructions (Millipore, USA). Histone H3 and Acetyl-Histone H3 Lys27 was obtained from Millipore. The ChIP primer sequences were listed in [Table S3](#). Quantification of immunoprecipitated DNA was performed using qPCR. ChIP data were calculated as a percentage relative to the input DNA by the Equation $2^{[\text{Input Ct} - \text{Target Ct}]} \times 0.1 \times 100$.

RNA immunoprecipitation (RIP)

A RIP assay was performed using the Magna RIP RNABinding Protein Immunoprecipitation Kit (Millipore, MA, USA) according to the manufacturer's instructions. Briefly, whole-cell extracts prepared in lysis buffer containing a protease inhibitor cocktail and RNase

inhibitor were incubated on ice for 5 minutes, followed by centrifugation at 10,000 g and 4°C for 10 minutes. Magnetic beads were preincubated with 5 µg of IP-grade antibody for 30 minutes at room temperature with rotation. The supernatant was added to bead-antibody complexes in immunoprecipitation buffer and incubated at 4°C overnight. Finally, the RNA was purified and quantified by qRT-PCR. Input controls and normal rabbit IgG controls were simultaneously assayed to ensure that the signals were detected from RNA that was specifically bound to protein.

RNA pulldown assay

Biotin-labeled RNA BDNF-AS was transcribed *in vitro* with the Biotin RNA Labeling Mix (Ambion) and T7 RNA polymerase (Ambion) and then treated with RNase-free DNase I (Ambion) and 0.5 M EDTA to stop the reaction.

Biotinylated RNAs were mixed with streptavidin magnetic beads (Life Technologies, Gaithersburg, MD) at 4°C overnight. Total cell lysates and RNase inhibitor were added to each binding reaction and incubated on ice for 1 hour. The RNA-protein binding mixture was boiled in SDS buffer, and the eluted proteins were detected by western blotting or mass spectrometry.

Cycloheximide (CHX) chase measurements of RNH1 half-life

The RNH1/his, BDNF-AS plasmids or BDNF-AS siRNA were transiently transfected into MCF-7 or MCF-7R cells. CHX (100 ng/ml) was added to the DMEM culture medium, and incubation was continued for the indicated hours. The cell lysates were submitted for western blotting using mouse anti-His monoclonal antibody (Invitrogen, Carlsbad, CA, USA), and western blot data were quantified using the ImageJ software.

mRNA decay measurements

The stability of the mTOR mRNA was assessed by adding 10 µg/ml actinomycin D into the cell culture medium to inhibit mRNA transcription. At the indicated time points, the relative amount of specific mRNA remaining in each sample could be correlated with mRNA degradation. Total RNA was extracted at indicated hours after actinomycin D (10 µg/ml) treatment, and the endogenous mTOR mRNA levels were analyzed by qRT-PCR. Since the mRNA levels for GAPDH were not changed after actinomycin D treatment, the GAPDH gene was used as a reference gene, and the ratio of mTOR and GAPDH in each sample was calculated.

Immunoprecipitation (IP) and ubiquitination assay

The RNH1/his, BDNF-AS plasmids or BDNF-AS siRNA were transiently transfected into MCF-7 or MCF-7R cells. 20 nM MG132 was added to the DMEM culture medium and incubation was continued for 5 hours. The lysates were immunoprecipitated with the indicated antibodies on protein A/G beads (Life Technologies) overnight at 4°C with rotation and were then boiled in SDS buffer. The eluted proteins were detected by western blotting.

Luciferase reporter assay

HeLa cells were seeded in 96-well plates at a density of 5000 cells per well. The cells were co-transfected with a mixture of 50 ng PGL3-basic-BDNF-AS promoter or PGL3-basic-BDNF-AS mutant promoter or other fragments, 10 ng Renilla and 50 ng pcDNA 3.1-MEF2A or control according to the recommended instructions by using the Lipofectamine 3000. After 48 hours of transfection, Firefly and Renilla luciferase activity was measured by the Dual-Luciferase Reporter Assay System (Promega). The relative firefly luciferase activities were detected, and Renilla luciferase activities served as an internal control.

RNA-CLIP

1×10^7 cells were cross-linked using 0.75% PFA (EMS-Fisher) and neutralized with 250 mM glycine. After being lysed with IP lysis buffer (Peirce) containing protease and RNase inhibitor, cells were scraped and sonicated. Precleared lysates were subjected to protein quantification using BCA, and an equal protein amount was included in each IP. In parallel, 5 µg antibody or IgG control were incubated with 40 µL Protein G Dynabeads (Invitrogen) overnight and then washed three times with IP lysis buffer. Precleared lysates were incubated with the bead conjugated antibodies overnight at 4°C. Beads were then eluted by gradient. After reversing the cross-link, RNA was then extracted from the eluates using TRIzol (Invitrogen), as described above. Immunoprecipitated RNAs were subjected to qPCR analyses.

Animal experiments

2×10^6 of MDA-MB-231 cells were orthotopically injected directly into the mammary fat pad of mice in 100 µL of sterile PBS. Once tumors reached 100 mm³, 10 mg/kg of BDNF-AS LNAs or LNA-Scramble (LNA 1: 5'-ATCGAGTCATCGCTGT-3', LNA 2: 5'-CGAA-CACGTGATAGAA-3', LNA Scramble: 5'-AACACGTCTATACGC-3') were intraperitoneally injected every 3 days for up to three weeks. Tumor volume was calculated every 3 days according to the formula $V (\text{mm}^3) = 0.5 \times (\text{length} \times \text{width}^2)$. Xenografts were harvested, weighed, and snap-frozen for cryosection when LNA treatments ended.

17β-Estrogen pellets (0.72 mg, 60-day release) were subcutaneously implanted 1 week before cell injection. 0.5×10^7 MCF-7 cells with doxycycline (DOX)-inducible wild-type or mutant BDNF-AS (loss of RNH1 binding motif) expression were implanted into the fat pads of nude mice. When tumor volume reached 100 mm³, mice were treated with subcutaneous implanted tamoxifen pellets, oral doxycycline (2 mg/ml) and oral Everolimus (5 mg/kg daily). Tumor volume was calculated every 3 days according to the formula V

(mm^3) = $0.5 \times (\text{length} \times \text{width}^2)$. Xenografts were harvested, weighed, and snap-frozen for cryosection when LNA treatments ended. The laboratory animal facility has been accredited by AAALAC (Association for Assessment and Accreditation of Laboratory Animal Care International) and the IACUC (Institutional Animal Care and Use Committee) of Guangdong Laboratory Animal Monitoring Institute approved all animal protocols used in this study.

QUANTIFICATION AND STATISTICAL ANALYSIS

All statistical analyses were performed using SPSS 20.0 software (IBM, SPSS, USA). The significance of differences between groups was estimated by Student's *t* test, χ^2 test or Wilcoxon test, as appropriate. Overall survival rates were calculated by the Kaplan–Meier method with the log-rank test applied for comparison. Survival data were evaluated using univariate and multivariate Cox proportional hazards model. Variables with a value of $p < 0.05$ in univariate analysis were used in subsequent multivariate analysis on the basis of Cox regression analyses. Two-sided *p-values* were calculated, and a probability level of 0.05 was chosen for statistical significance.